Office of Naval Research

Contract N50RI-76 • Task Order No. 1 • NR-071-012

THE COLLINEAR ANTENNA ARRAY WITH A SECTION OF TWO-WIRE LINE AS COUPLING ELEMENT

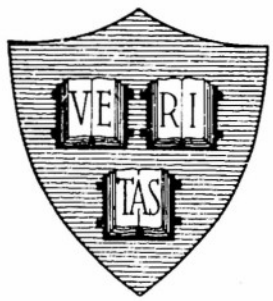

By

Charles C. H. Tang

May 1.1954

Technical Report No. 196

Cruft Laboratory
Harvard University
Cambridge, Massachusetts

Office of Naval Research

Contract N5ori-76

Task Order No. 1

NR-078-011

Technical Report

on

The Collinear Antenna Array with a Section of Two-Wire Line as Coupling Element

by

Charles C. H. Tang

May 1, 1954

The research reported in this document was made possible through support extended Cruft Laboratory, Harvard University, jointly by the Navy Department (Office of Naval Research), the Signal Corps of the U. S. Army and the U. S. Air Force, under ONR Contract N5ori-76, T. O. 1.

Technical Report No. 196

Cruft Laboratory

Harvard University

Cambridge, Massachusetts

A list of Cruft Laboratory Technical Reports

is available on request.

TR196

The Collinear Antenna Array with a Section of Two-Wire Line as Coupling Element

by

Charles C. H. Tang

Cruft Laboratory, Harvard University

Cambridge, Massachusetts

Abstract

The problem of a symmetrical three-element collinear antenna array with a section of two-wire line as the coupling element between antennas is studied in order to obtain qualitatively the conditions under which the currents in the parasites are in phase with the currents in the driven antenna. The phase of the currents in the parasitic elements is reversed only when (1) the overall length of the section of two-wire line and the parasite is near an odd integral multiple of a quarter-wavelength, and (2) the position of the short-circuiting bar or tandem bridge on the section of line is about a quarter-wavelength away from the array. The reversal of the phase of the current on the parasite is independent of the length of the driver, but the length of the driver is involved in the driving-point impedance. The current on the array as a whole can be decomposed into a main antenna current and a secondary antenna current. The main antenna current due to the driving voltage is excited on the driver and the two-wire line, while the gap voltage produced indirectly by the main antenna current is responsible for the secondary antenna current on the driver and parasite. It is the secondary antenna mode that causes the reversal of the phase of the current on the parasite. The radiation field of the array as a whole is a superposition of the two-fields produced respectively by the current on the two-wire line and that on the driver and parasites.

- - - - - - - - - -

The analysis of the collinear antenna array of three elements has been carried out by King [1] and by Andrews [2] using a different approach. King [3] also made an approximate analysis of the collinear antenna array with a two-wire line as coupling element. A general quantitative analysis of the problem of the collinear antenna array with two-wire line as coupling element is necessarily very complicated, since in addition to the parameters, thickness and length,

for a simple dipole antenna it has the following extra parameters: number and length of parasites, spacing between the driver and the parasite, length of the two-wire line, and the position of the short-circuiting bar on the two-wire line. The presence of the two-wire line in a direction perpendicular to the array introduces extra complexity on coupling effects among the elements of the array, and the problem becomes a two-dimensional one.

The purpose of utilizing the two-wire line as a coupling element lies in an attempt to reverse the phase of the current on the parasites so as to obtain a field pattern similar to that produced by a simple collinear array with its individual units center-driven with inphase currents of approximately the same magnitude. Such is not the case as will be discussed later, since the presence of the two-wire line in a direction perpendicular to the array essentially introduces a field pattern in space quadrature with that of the array alone. This is due to the fact that codirectional antenna currents exist on the two-wire line and contribute significantly to the distant field. In fact, the problem is similar to that of an antenna with a right-angle bend, and a mathematical analysis of an antenna with a right-angle bend is not yet available.

To obtain an overall picture of the characteristics of the array, measurements are presented in this report that cover various combinations of the parameters mentioned above. The length of the parasite has been fixed at a half-wavelength for all measurements, since this is the length of practical importance and interest.

The equipment used for the measurements is described in Technical Report No. 177. It consists of an image screen and a driving coaxial line with suitable probes to measure the current distribution on the antenna and in the driving line. The frequency is 600 Mc/s. The inside diameter of the outer conductor of the coaxial line is 2.032 in., and the diameter of the inner conductor or antenna is 1/4 in. The characteristic impedance of the line is 123.6 Ω, and it has a phase constant of 12.775 rad/m and a theoretical attenuation of 0.003 nepers/m. Figure 1 shows a block diagram of the circuit used, and Fig. 2 shows the actual arrangement of the equipment. The diameter of the antenna used in the measurements is 1/4 in. The section of two-wire line used as a coupling element has a diameter of 1/16 in. and

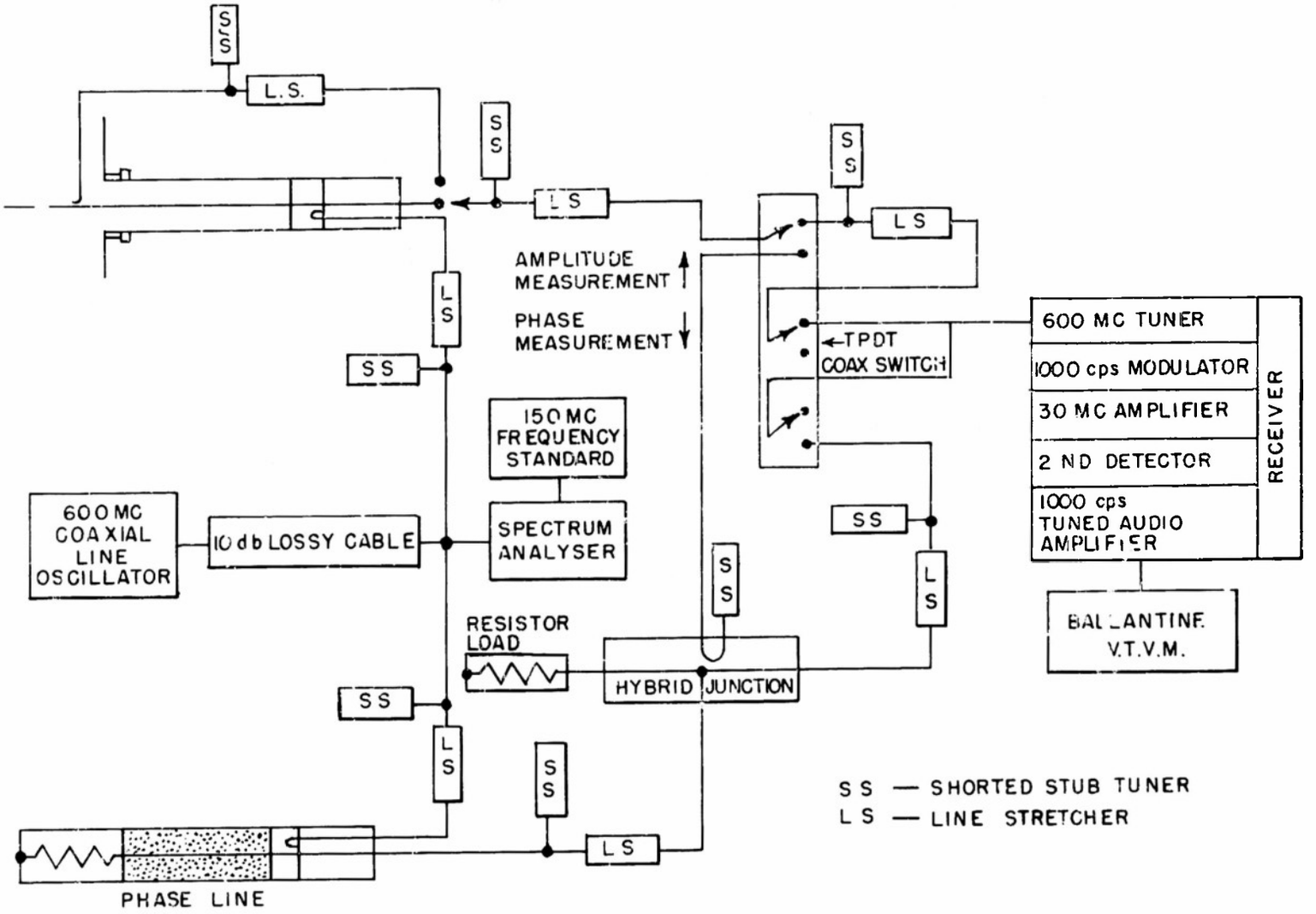

FIG.I BLOCK DIAGRAM OF EXPERIMENTAL EQUIPMENT

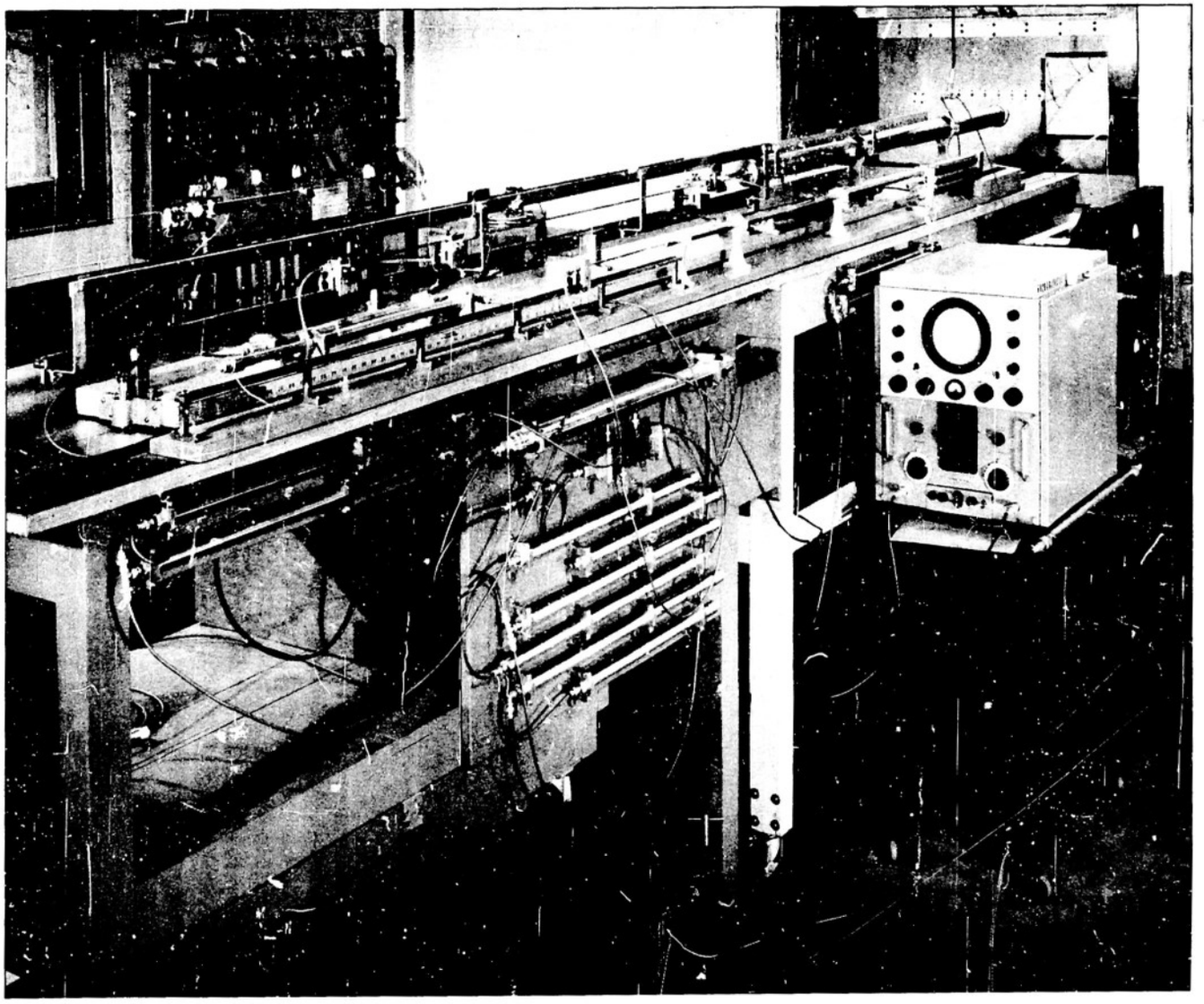

FIG. 2 MEASURING LINE AND JUNCTION BOARD

a spacing of 1/2 cm ($\frac{1}{100}\lambda$) which satisfies the condition $\beta_o b \ll 1$ in order to prevent significant radiation from the balanced mode on the two-wire line. The two-wire line for these dimensions has a characteristic impedance of 220 Ω. The short-circuiting bar used on the two-wire line is of tandem-bridge type in order to isolate the balanced mode within the short-circuited portion of the two-wire line.

Figure 3 shows the measured impedance for lengths of two-wire line of 25 cm ($\frac{1}{2}\lambda$), 33 cm, and 37.5 cm ($\frac{3}{4}\lambda$) with the position of the short-circuiting bar or tandem bridge on the two-wire line as the variable parameter. Figure 4 shows the phase and amplitude of the current at the center of the parasite relative to that near the driving point. The exact magnitude and phase of the current at the driving point can not be measured directly by the auxiliary current probe due to physical difficulties; however, they can be obtained by extrapolation with the aid of the main current probe inside the driver antenna. The method of the extrapolation has not been used since it involves a considerable amount of labor and, in addition, the results may not be accurate. Since only the relative change of the magnitude and phase of the current on the parasite with respect to that on the driver is of interest, the choice of reference point on the driver and parasite is not critical, so long as the reference point is maintained throughout the measurements. The curves of normalized current shown in Fig. 4 yield an excellent picture of the relative change of the current at the parasite to that on the driver. All the measured points fit rather smoothly on circles, and the position of the circles rotates in clockwise direction as the length of the two-wire line increases. It is seen that the phase of the current on the parasite does reverse when (1) the total length of the parasite and two-wire line is near an odd multiple of quarter-wavelength, and (2) the short-circuiting bar is placed about a quarter-wavelength away from the array. For lengths other than that near an odd multiple of a quarter-wavelength, the phase of the current on the parasite never reverses regardless of where the short-circuiting bar is placed. When the short-circuiting bar is placed about a half-wavelength away from the end at the antenna, the current on the parasite is about 180 degrees out of phase to that on the driver for all lengths of the two-wire line.

From both Fig. 3 and Fig. 4 it is seen that the variations of current

and impedance are relatively small when the total length of the parasite and two-wire line is a multiple of half-wavelength. The interpretation of these measured results can be made clearer with the aid of Fig. 5. Consider the configuration if Fig. 5(a) where the length of the two-wire line is $\frac{3}{4}\lambda$, and the position of the short-circuiting bar is $\frac{1}{4}\lambda$ away from the array. Because of the presence of the two-wire line, the quarter-wavelength driver is effectively lengthened by an amount equal to the length of the two-wire line, and consequently the array as a whole has a main antenna current oscillating around a right-angle-bended antenna with the bend a quarter-wavelength away from the image plane. This main antenna current is schematically shown, without considering mutual action due to the bend, by full lines in Figs. 5(a), (b), (c), (d). A justification of the above statement is necessary because the presence of the parasite must be taken into consideration. The parasite does play an important role in changing the characteristics of the array as a whole; however, its effect on the driver is entirely different from that of the two-wire line. Because the parasite is not directly connected to the driver, but directly connected to the two-wire line, the coupling between the driver and the parasite is similar to that of a simple three-element collinear array. The presence of the half-wavelength parasite does not significantly change the distribution and magnitude of the current on the driver. On the other hand, the presence of the two-wire line drastically alters the distribution and magnitude of the current on the driver.

The current induced on the parasite is partly due to the coupling from the antenna current on the driver and partly due to the direct coupling from the antenna current on the two-wire line. These two couplings to the parasite are present all the time, but the distribution and magnitude of the induced current on the parasite are determined mainly by the total length of the parasite and two-wire line. This is due to the fact that any induced current on the parasite must surge through the two-wire line since the two-wire line is directly connected to the parasite. Accordingly, if the total length of the parasite and two-wire line is nearly self-resonant, a very strong oscillation will be produced on them. This self-resonant current on the parasite and two-wire line is shown by dashed lines in Figs. 5(b) and (d). On the other hand, if the total length is near a detuning length, the induced current on the para-

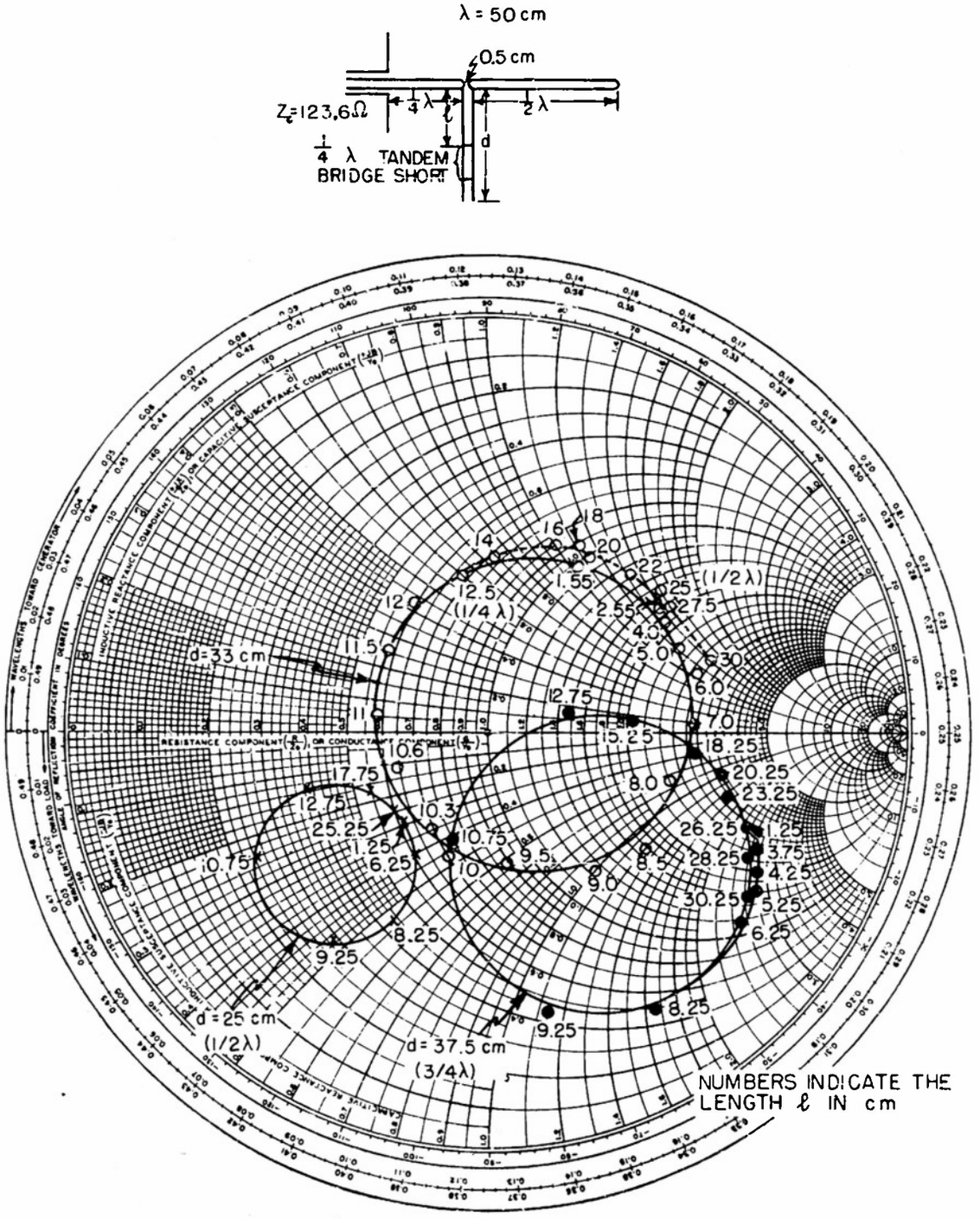

FIG 3 MEASURED IMPEDANCE OF THE COLLINEAR ARRAY WITH TWO-WIRE LINE AS COUPLING ELEMENT

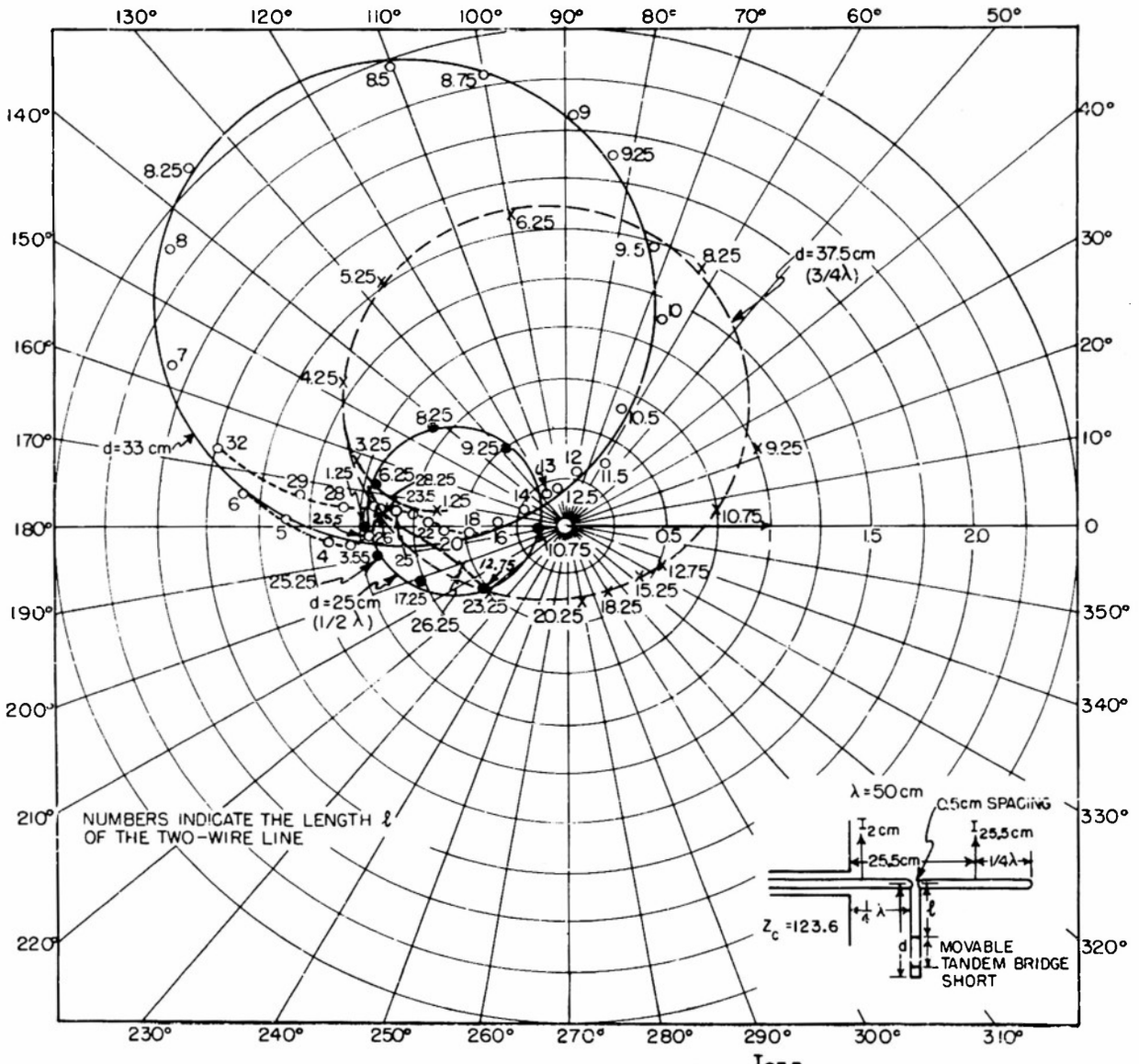

FIG. 4 NORMALIZED CURRENT RATIO $\frac{I_{25.5}}{I_2}$

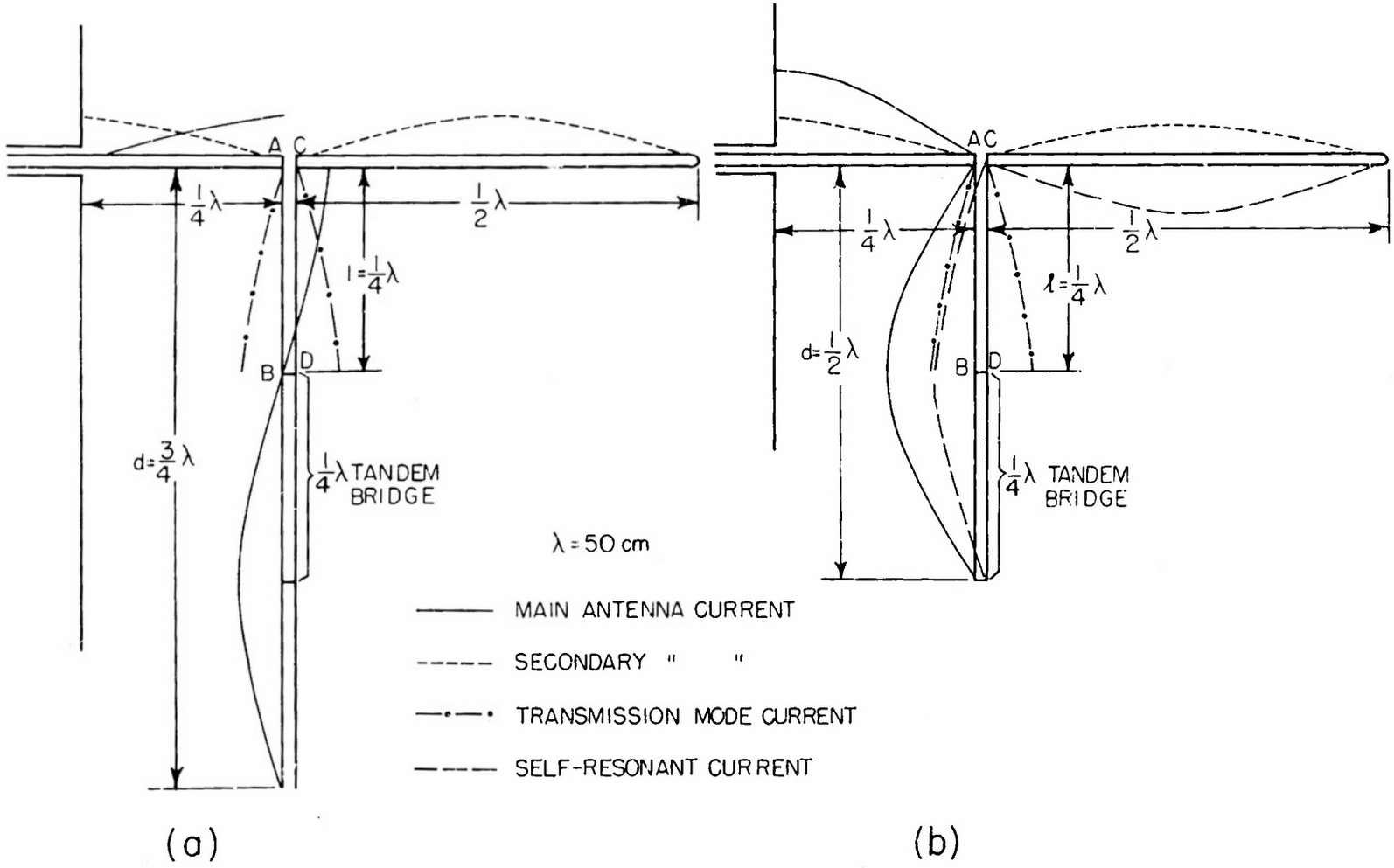

FIG. 5 SCHEMATIC DISTRIBUTION OF COMPONENT CURRENTS

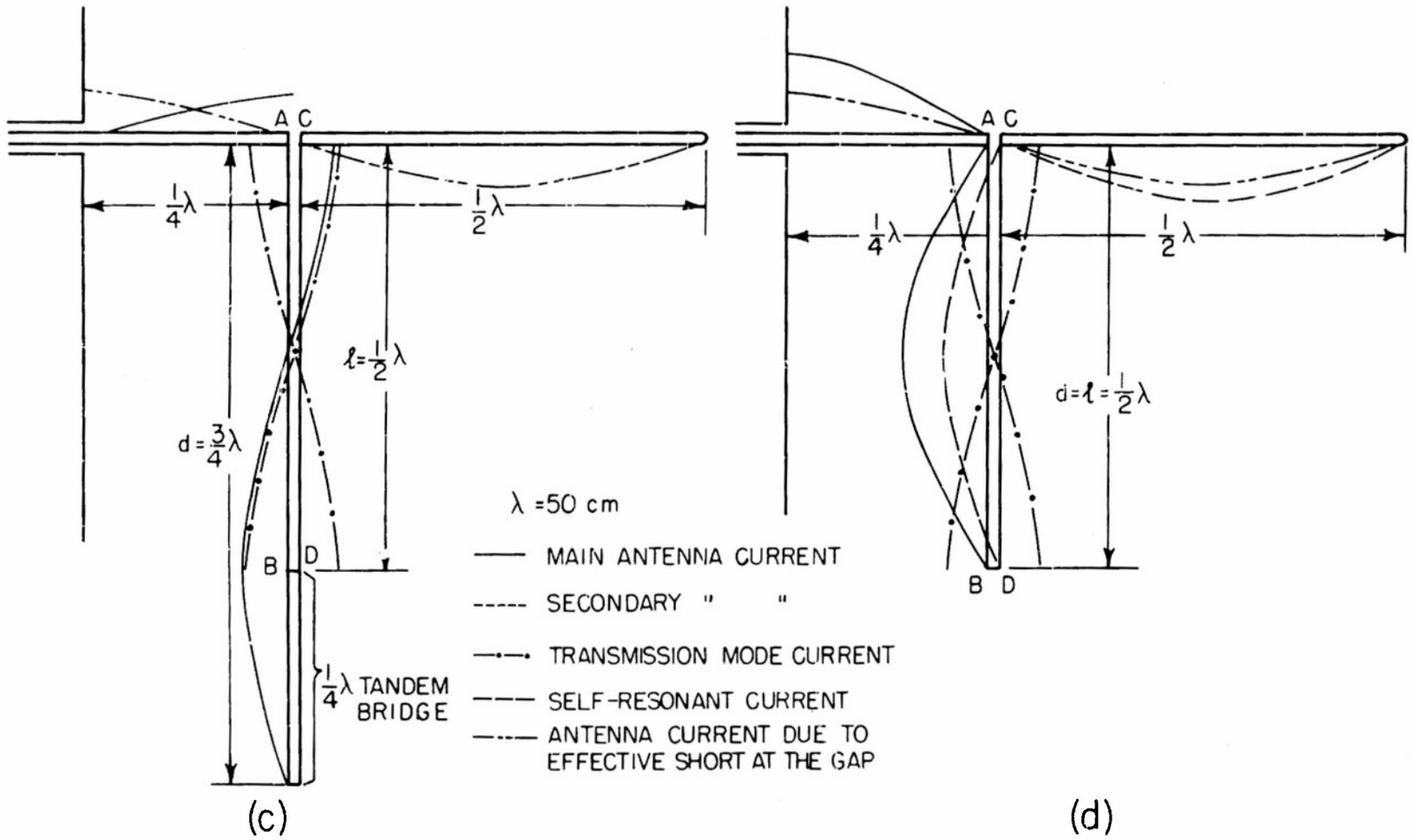

FIG. 5 SCHEMATIC DISTRIBUTION OF COMPONENT CURRENTS

site and two-wire line will be negligible. Figures 5(a) and (c) show such cases.

It is now necessary to analyze the mechanism by which the balanced mode is produced on the short-circuited section of the two-wire line. From Fig. 5 it is seen that the end A of the two-wire line is in contact with the driver, while the end C is not. As the main antenna current begins to oscillate on the driver and two-wire line, that part of the antenna current on section AB of the two-wire line will induce an e.m.f. in section CD in such a direction as to produce a current of proper magnitude to oppose that in AB. This induced current on CD will in turn induce an opposite current in AB, and this mutual induction proceeds until equilibrium is reached. Therefore, in the short-circuited section ABCD of the two-wire line a balanced mode (shown by dash-and-dot line in Fig. 5) is set up, and a voltage exists between opposite points on AB and CD. There is, of course, a voltage existing between the gap or between the points A and C. Since the short-circuiting bar is placed at BD, according to transmission-line theory BD must be at current maximum or voltage minimum. The gap voltage will be a maximum, if the short-circuited section is about $\frac{1}{4}\lambda$ in length as shown in Figs. 5(a) and (b). It will be a minimum if the short-circuited section is about $\frac{1}{2}\lambda$ in length as shown in Figs. 5(c) and (d). Since the balanced mode on the two-wire line is not exactly sinusoidal due to nonsinusoidal antenna current, the gap voltage may not be exactly a maximum with the short-circuiting bar placed $\frac{1}{4}\lambda$ away from the gap. It is important to notice that there is no balanced mode on the free-end section of the two-wire line. The free-end section simply presents itself as a section of antenna which is thicker than the section AB.

As a result of the presence of the gap voltage, a secondary antenna current is produced in the driver and the parasite. In fact, this configuration is that of an off-center-driven dipole erected over an image plane. This case has been analyzed by Taylor [4] and the actual distribution of current depends upon the lengths of the driver and the parasite. For the configuration of Fig. 5 the actual current distribution is not as simple as that shown by dotted lines in Fig. 5, but Fig. 5 is a good approximation. The important point is that the currents in the driver and parasite at corresponding points (with gap as point of symmetry) have approximately the same phase and magnitude. It

is this secondary antenna current which is responsible for the reversal of the current on the parasite. For the configuration of Fig. 5(a) the significant current present on the parasite is the secondary antenna current due to gap voltage, since the induced current on the parasite and two-wire line is small as a result of the detuning effect of the over-all length. The current on the driver is the algebraic sum of the main antenna current and secondary antenna current. The phase and magnitude of the secondary antenna current due to gap voltage depends upon the position of the short-circuiting bar, while the magnitude and phase of the main antenna current due to driving voltage are approximately constant for fixed length of the two-wire line. For the configuration of Fig. 5(a) the current on the parasite is approximately in phase with that on the driver.

According to the preceding discussion, there should be no current on the parasite for the arrangement of Fig. 5(c) since the gap voltage is a minimum or zero for $\ell = \frac{1}{2}\lambda$. However, it should be noticed that the gap is effectively short-circuited for $\ell = \frac{1}{2}\lambda$ as if the parasite were directly connected to the driver. As a result an antenna current (double-dashed and double-dotted line) due to driving voltage will be produced on the driver and the parasite as a continuous antenna. In fact, for this case the two-wire line and the parasite are connected in parallel at the gap point. The impedance looking in at the gap point is very low, because the $\frac{3}{4}\lambda$ two-wire line antenna of low impedance is connected in parallel with $\frac{1}{2}\lambda$ parasite of high impedance. Accordingly, the input impedance at the driving point is high since the driver is $\frac{1}{4}\lambda$ in length. This checks very well with the measured point as seen from Fig. 3 for $d = \frac{3}{4}\lambda$ and $\ell \doteq \frac{1}{2}\lambda$.

For the configurations of Figs. 5(b) and (d) the self-resonant current on the parasite and two-wire line is large. The secondary antenna current produced on the parasite because of maximum gap voltage (Fig. 5(b)) is able to cancel only a part of the self-resonant current on the parasite, and therefore the current on the parasite never reverses its phase. This effect is clearly indicated in Fig. 3 for the impedance and in Fig. 4 for normalized current. The circles for d = 25 cm ($\frac{1}{2}\lambda$) in both figures are small in comparison with circles for other lengths of d, indicating that the variations of current and impedance are small when ℓ is varied. In particular, the current ratio circle

does not enclose the origin, indicating that the current on the parasite is never in phase with that on the driver. A series of current-distribution curves and phase-variation curves for the configuration of quarter-wavelength driver, half-wavelength parasite, 33 cm two-wire line, and different position of short-circuiting bar on the two-wire line are shown in Fig. 6 to Fig. 9 respectively. The crosses in these figures are the measured current points obtained by the main current probe, and they serve as a guide in extrapolating the measured current points obtained by the auxiliary probe into the region near the driving point. Good correlation can be seen by comparing these curves with the current curve for d = 33 cm in Fig. 4.

The preceding measurements and analysis used a driver of quarter-wavelength and a parasite of half-wavelength over the image plane, and this configuration with its image is equivalent to a three-half-wave-element array with two-wire lines as coupling elements. If a driver of half-wavelength is used instead, the equivalent of a four-half-wave-element array results. Figure 10 shows the normalized ratio of the current at the center of the parasite to that at the center of the driver for a half-wavelength driver and a half-wavelength parasite, and Fig. 11 shows the corresponding driving point impedance. Again it is seen that the current on the parasite reverses its phase when the total length of the parasite and two-wire line is near an odd multiple of a quarter-wavelength. The variations of driving-point impedance and normalized current ratio are small when the total length of the parasite and two-wire line is near a multiple of a half-wavelength. The interpretation of these measured results is exactly the same as that for the quarter-wavelength driver case, and it can be facilitated by using Fig. 12. It can be concluded, therefore, that it is the total length of the parasite and two-wire line that determines the phase reversal of the current on the parasite, and the length of the driver plays an insignificant part in phase reversal. The length of the driver, however, plays an important role in characterizing the driving-point impedance and field pattern of the array. This can be seen by comparing Fig. 11 with Fig. 3. The impedance looking at the gap for the arrangement of Fig. 12(c) is very low, because the $\frac{3}{4}\lambda$ two-wire line of low impedance is effectively connected in parallel with $\frac{1}{2}\lambda$ parasite of high impedance. Thus the impedance looking at the driving point must be also very low due to the fact that the driver is a half-wavelength in this case. This result also checks with the measured impedance

as seen from Fig. 11 for the circle d = $\frac{3}{4}\lambda$, since the point for $\ell \doteq 25$ cm($\frac{1}{2}\lambda$) does lie in the low-impedance region of the circle. Figure 13 shows the current distribution for the configuration of a half-wavelength driver, half-wavelength parasite, and $\frac{3}{4}\lambda$ two-wire line with shorting bar placed at ℓ = 1.25 cm (almost equivalent to $\ell \doteq \frac{1}{2}\lambda$). For this position of the short-circuiting bar the gap voltage is very small, since it is almost an equivalent short circuit at the gap. The current maximum at the end of the driver is expected, as the current on the driver is dominated by the antenna current on the low-impedance, right-angle-bended antenna composed of the driver ($\frac{1}{2}\lambda$) and the two-wire line ($\frac{3}{4}\lambda$). This measured current distribution is in agreement with the schematic diagram of Fig. 12(c).

The analysis in the preceding paragraphs can be summarized with simplications by saying that on the array as a whole a constant antenna mode (on the driver and the two-wire line of fixed length) due to the driving voltage is superimposed on a secondary antenna mode due to a gap voltage the magnitude of which depends on the position of the short-circuiting bar on the two-wire line. The change of the position of the short-circuiting bar apparently does not affect the magnitude and distribution of the antenna mode on the driver and the two-wire line, as the change of position of the short-circuiting bar does not alter the length of the two-wire line.

If the short-circuiting bar is fixed permanently at the free end of the two-wire line and the length of the short-circuited two-wire line is varied, a different situation results. In this case, both the antenna mode on the driver and two-wire line due to driving voltage, and the secondary antenna mode due to gap voltage vary simultaneously as the length of two-wire line with a short-circuit at the free end is varied. The measured input impedance curve and the normalized current curves for such a configuration are in Fig. 14 and Fig. 15 respectively. Comparison of these curves with those in Fig. 3 and Fig. 4 shows they are quite different in shape; however, the current on the parasite does reverse its phase as in the previous configurations only for lengths of two-wire line that are near an odd multiple of a quarter-wavelength (for $\frac{1}{2}\lambda$ parasite case). The analysis used above is also valid for such a configuration. Figures 16-18 show respectively the current distributions and phase variations for three different lengths of two-wire line shorted

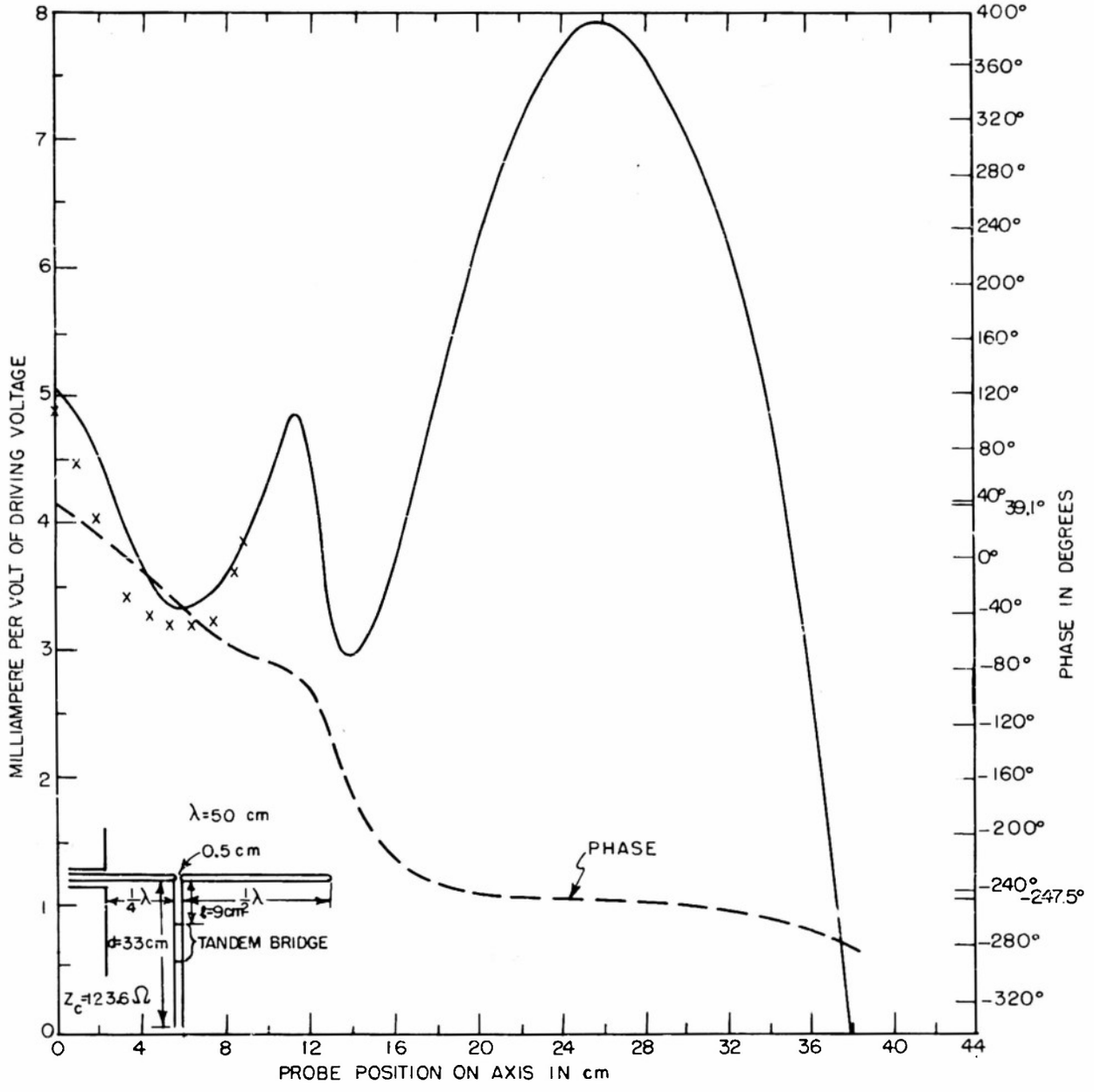

FIG. 6 MEASURED CURRENT DISTRIBUTION AND PHASE VARIATION

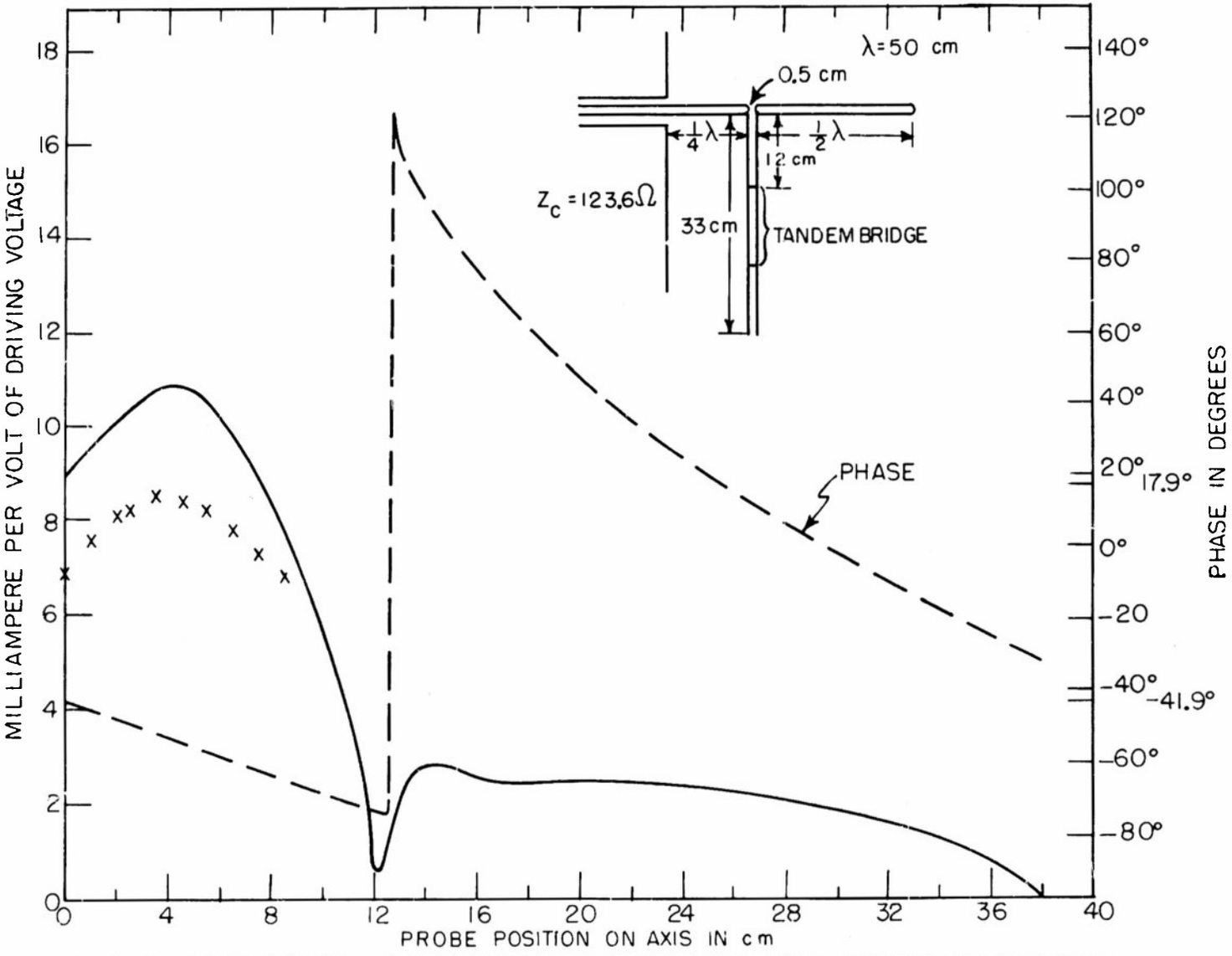

FIG. 7 MEASURED CURRENT DISTRIBUTION AND PHASE VARIATION

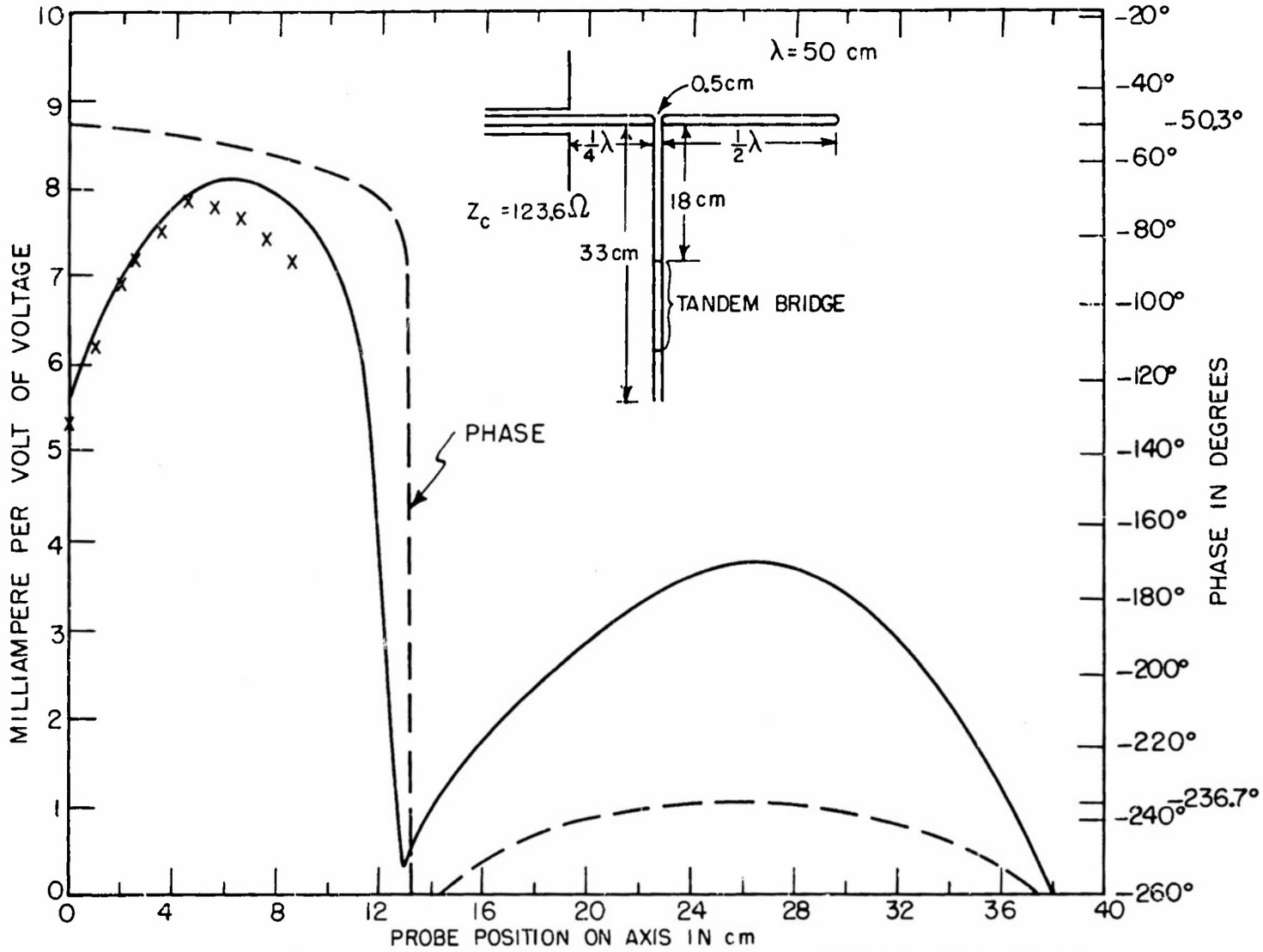

FIG.8 MEASURED CURRENT DISTRIBUTION AND PHASE VARIATION

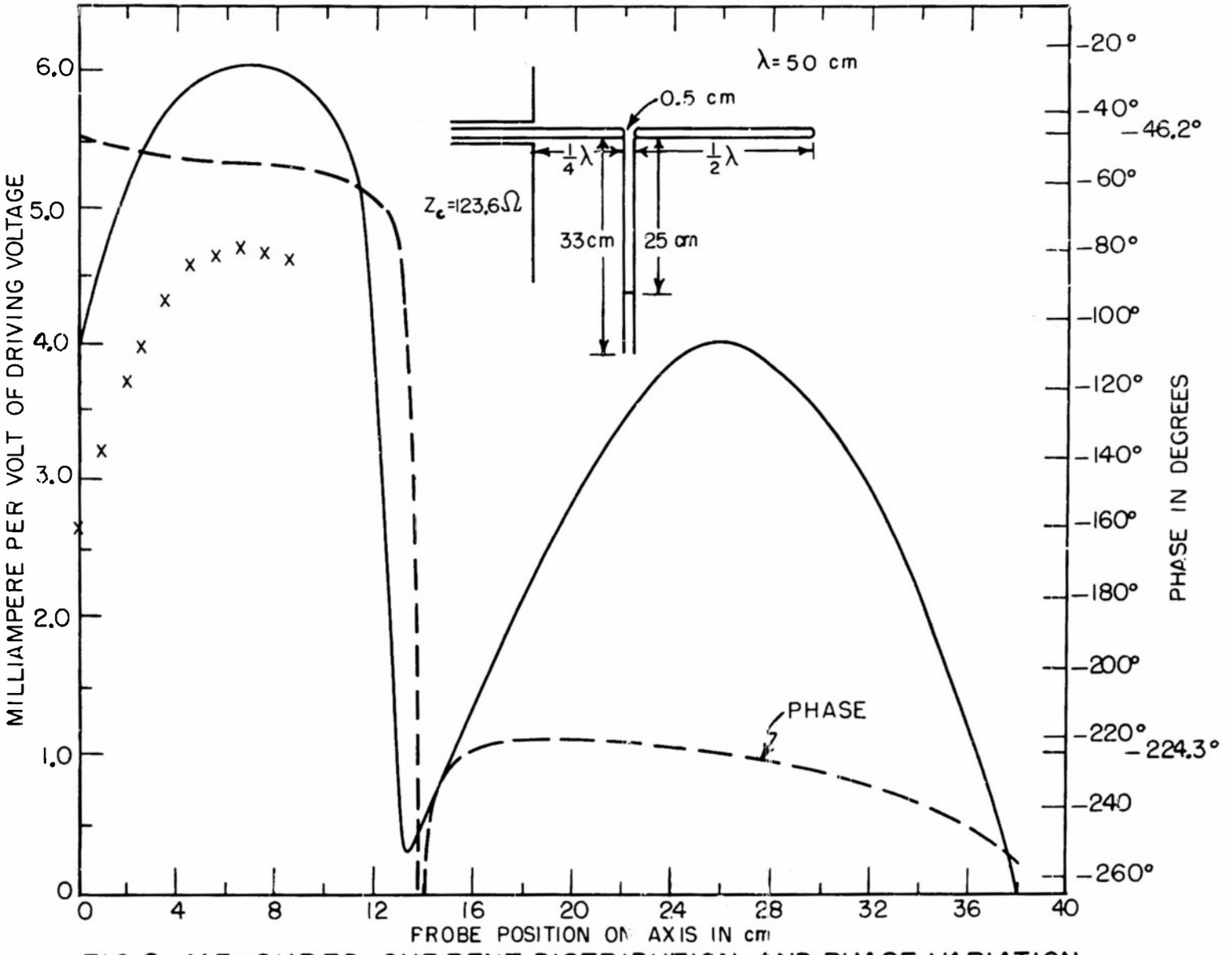

FIG. 9 MEASURED CURRENT DISTRIBUTION AND PHASE VARIATION

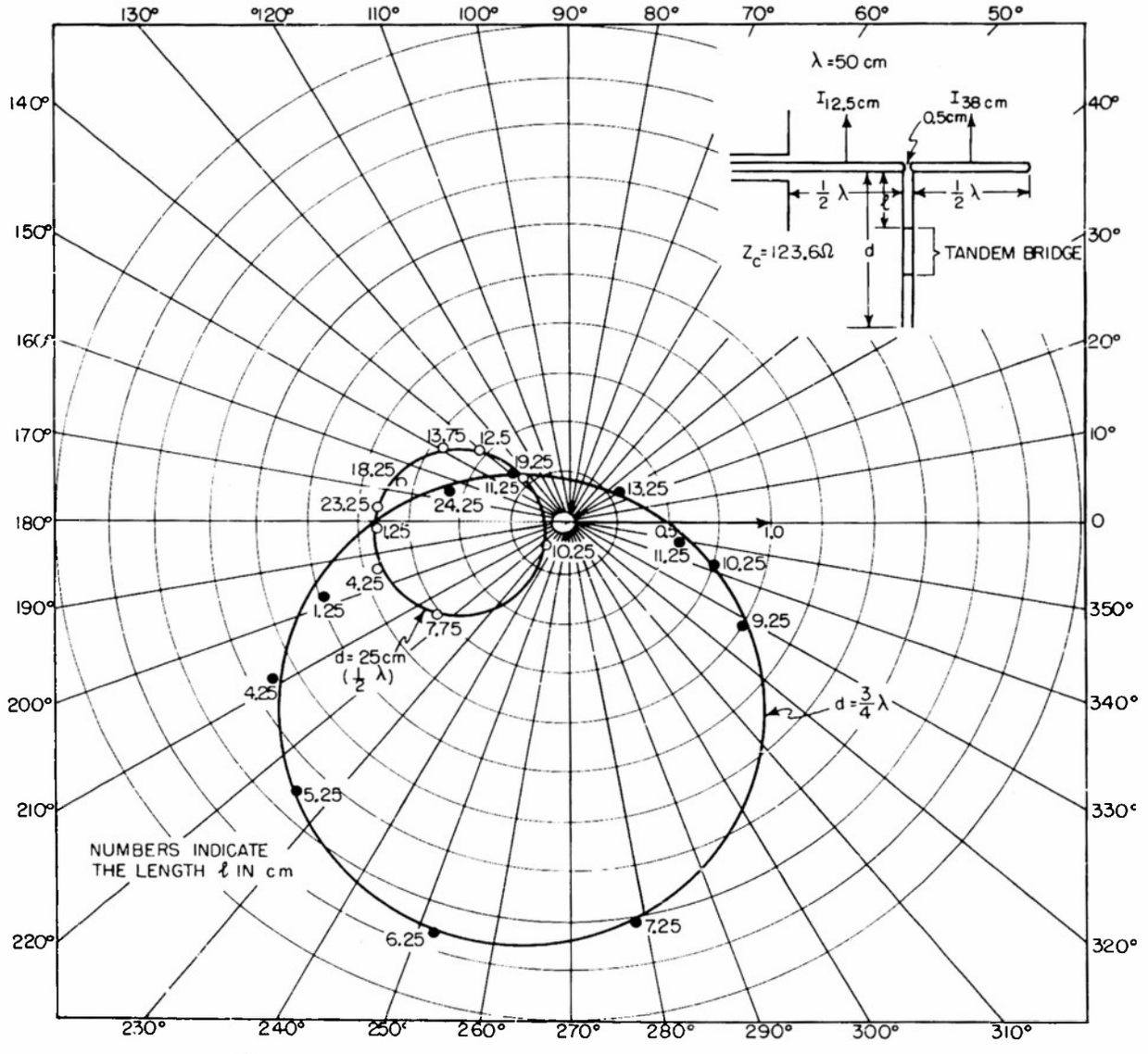

FIG. 10 NORMALIZED CURRENT RATIO $\frac{I_{38}}{I_{12.5}}$

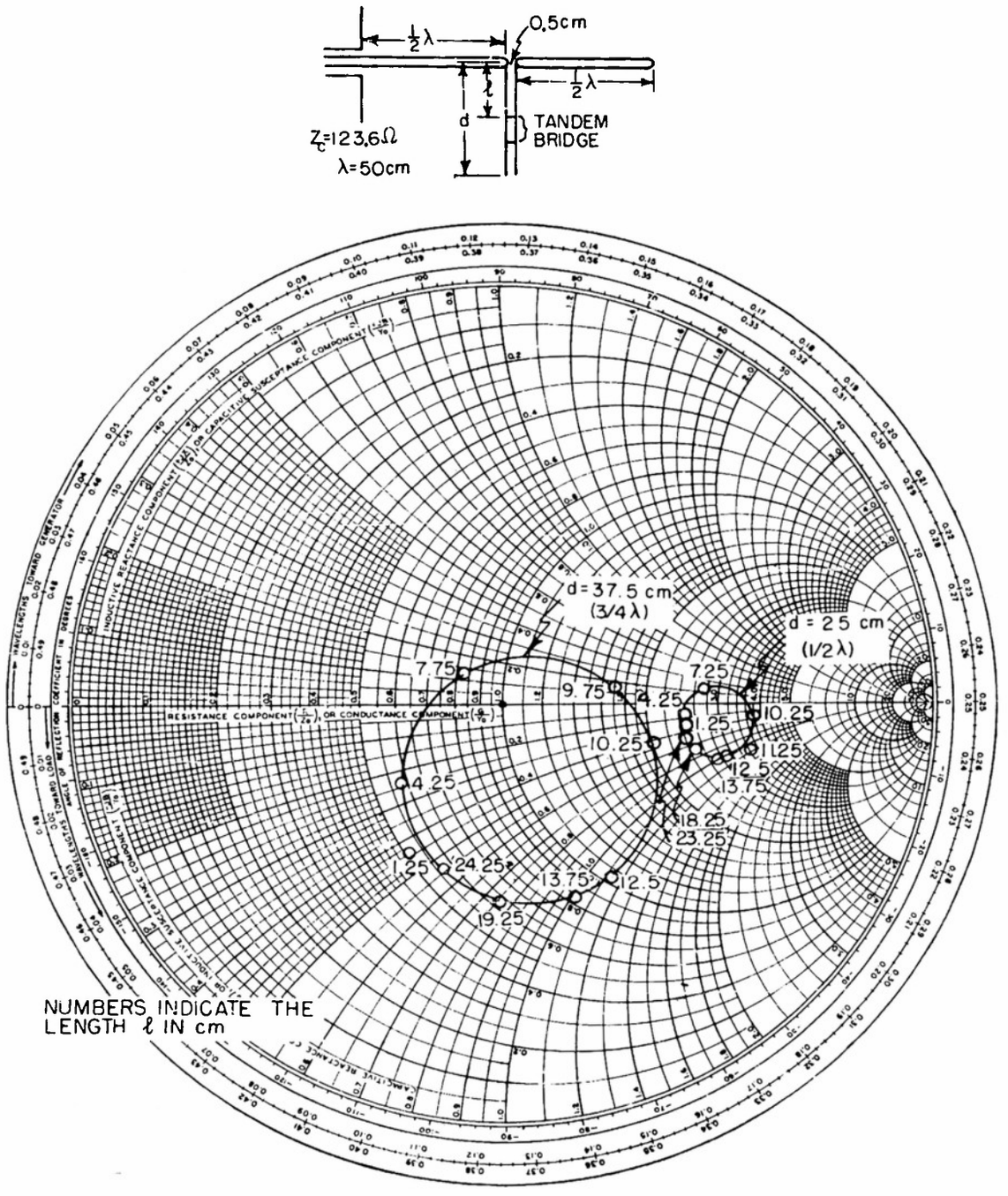

FIG.11 MEASURED IMPEDANCE OF THE COLLINEAR ARRAY WITH TWO-WIRE LINE AS COUPLING ELEMENT

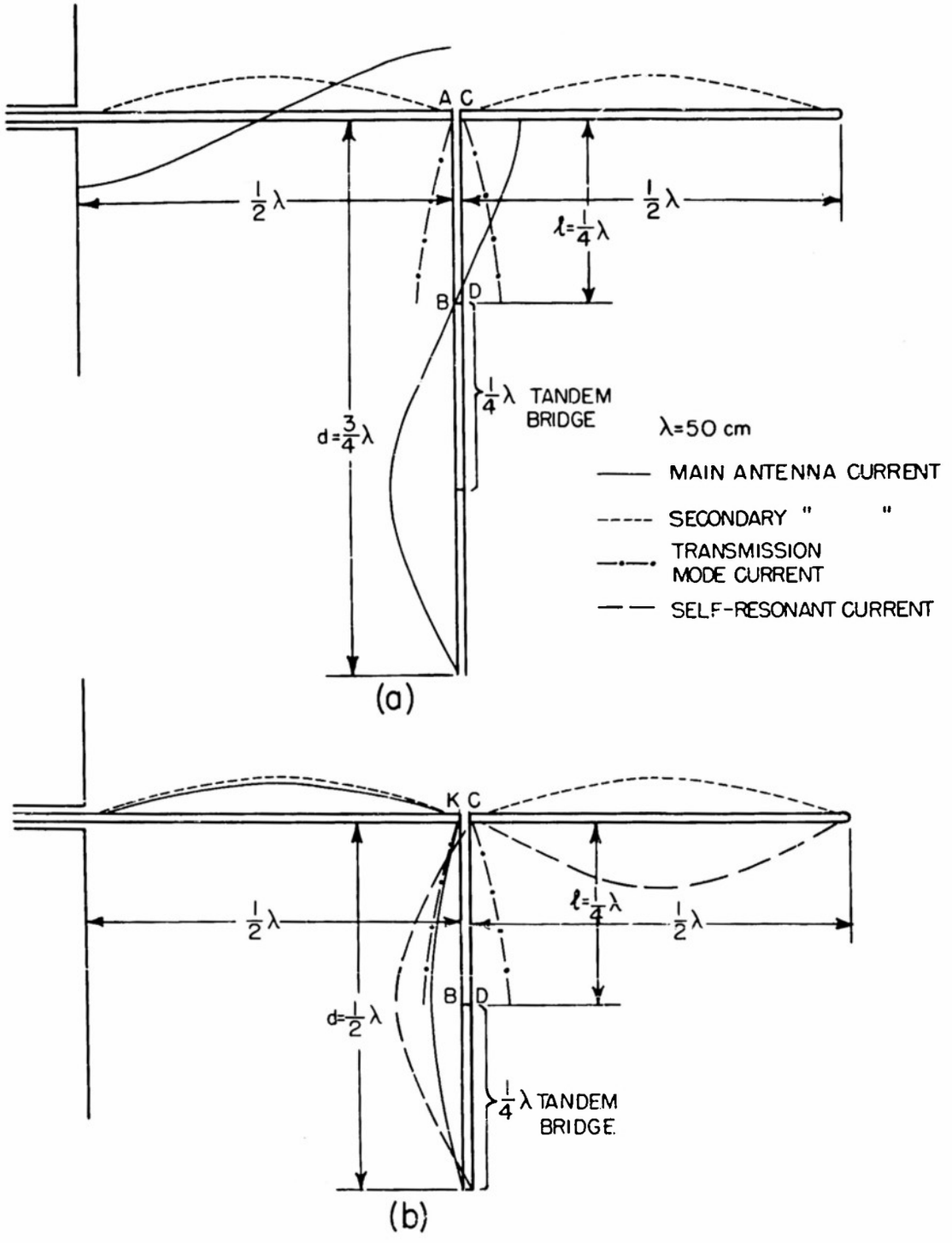

FIG. 12 SCHEMATIC DISTRIBUTION OF COMPONENT CURRENTS

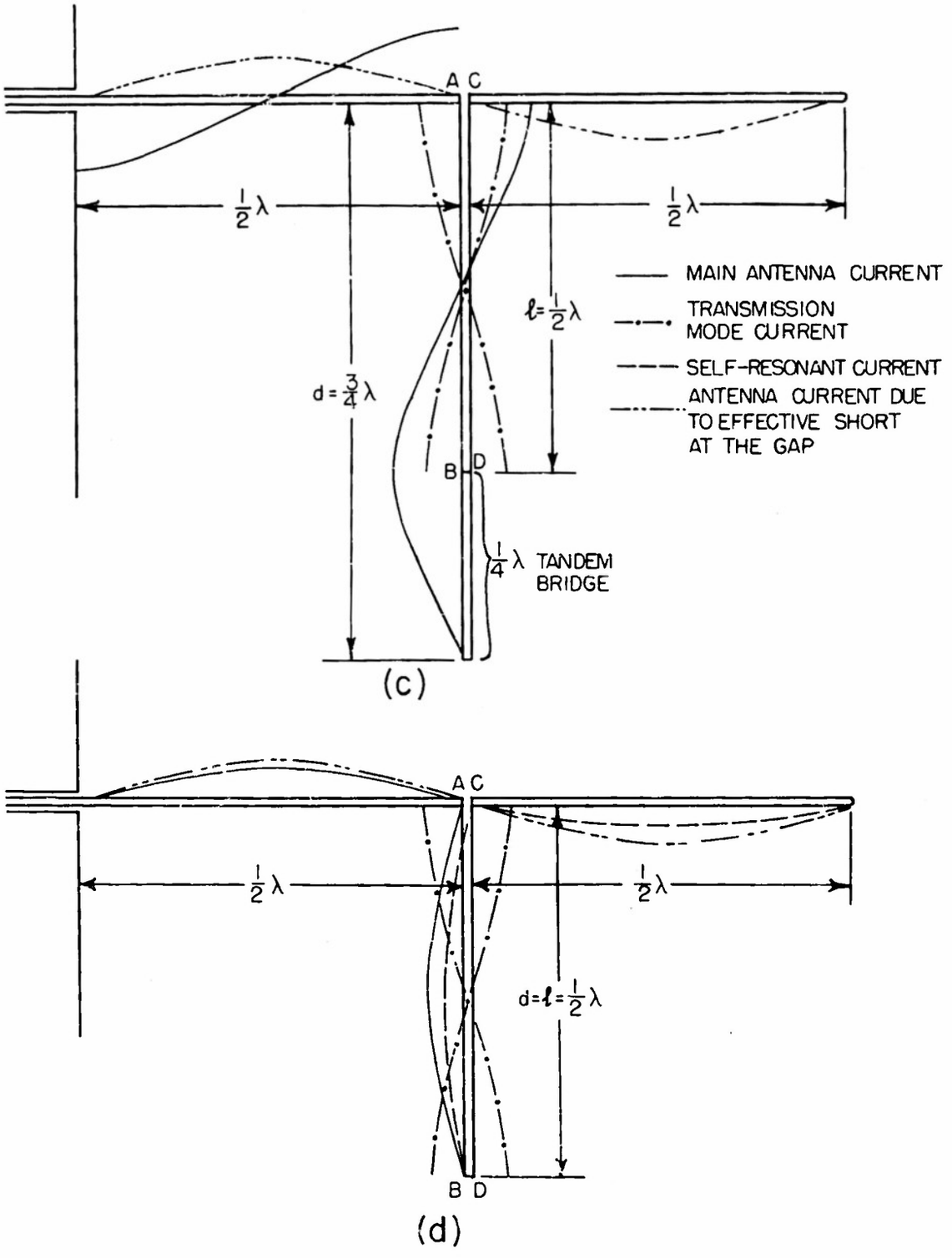

FIG. 12 SCHEMATIC DISTRIBUTION OF COMPONENT CURRENTS

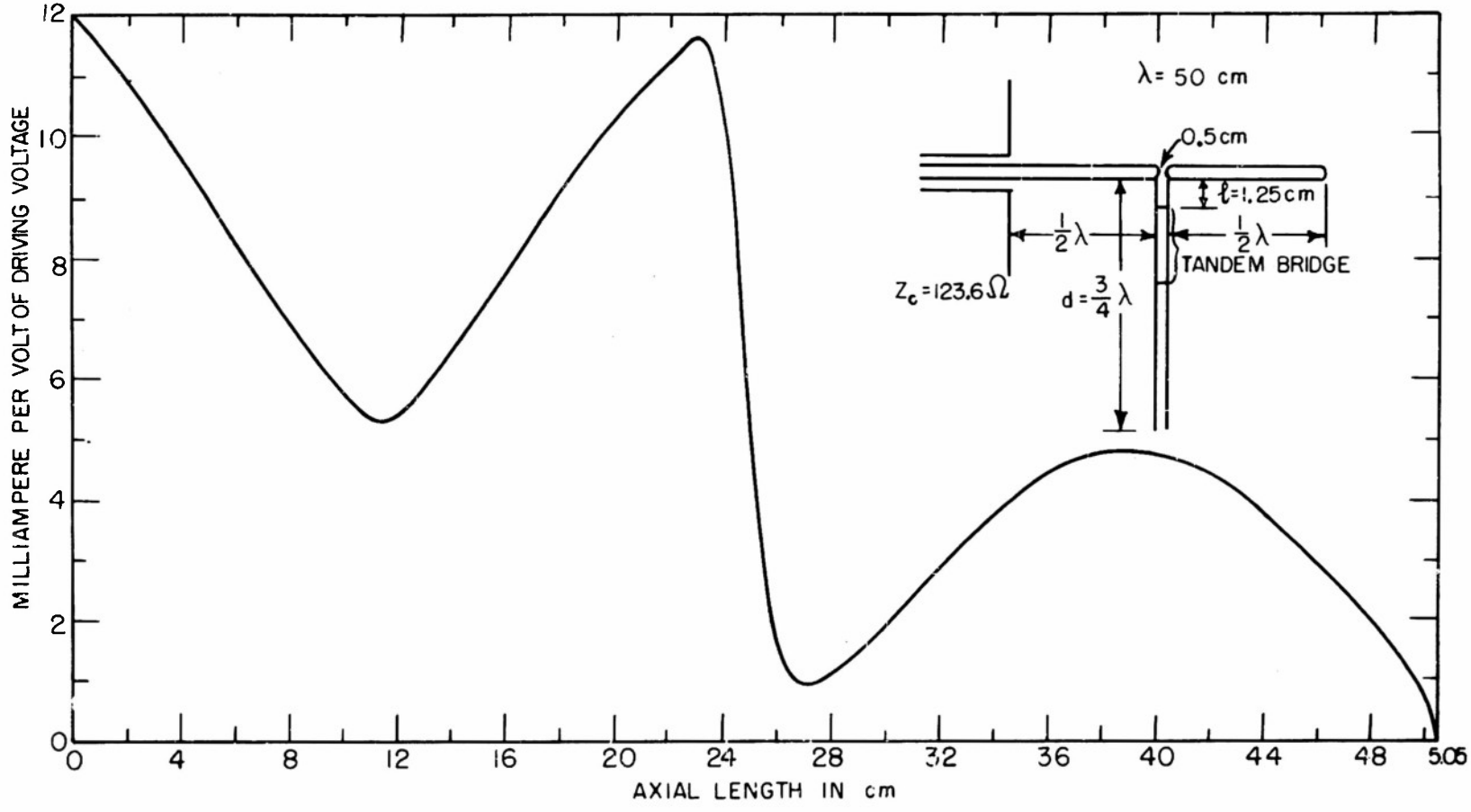

FIG.13 MEASURED CURRENT DISTRIBUTION

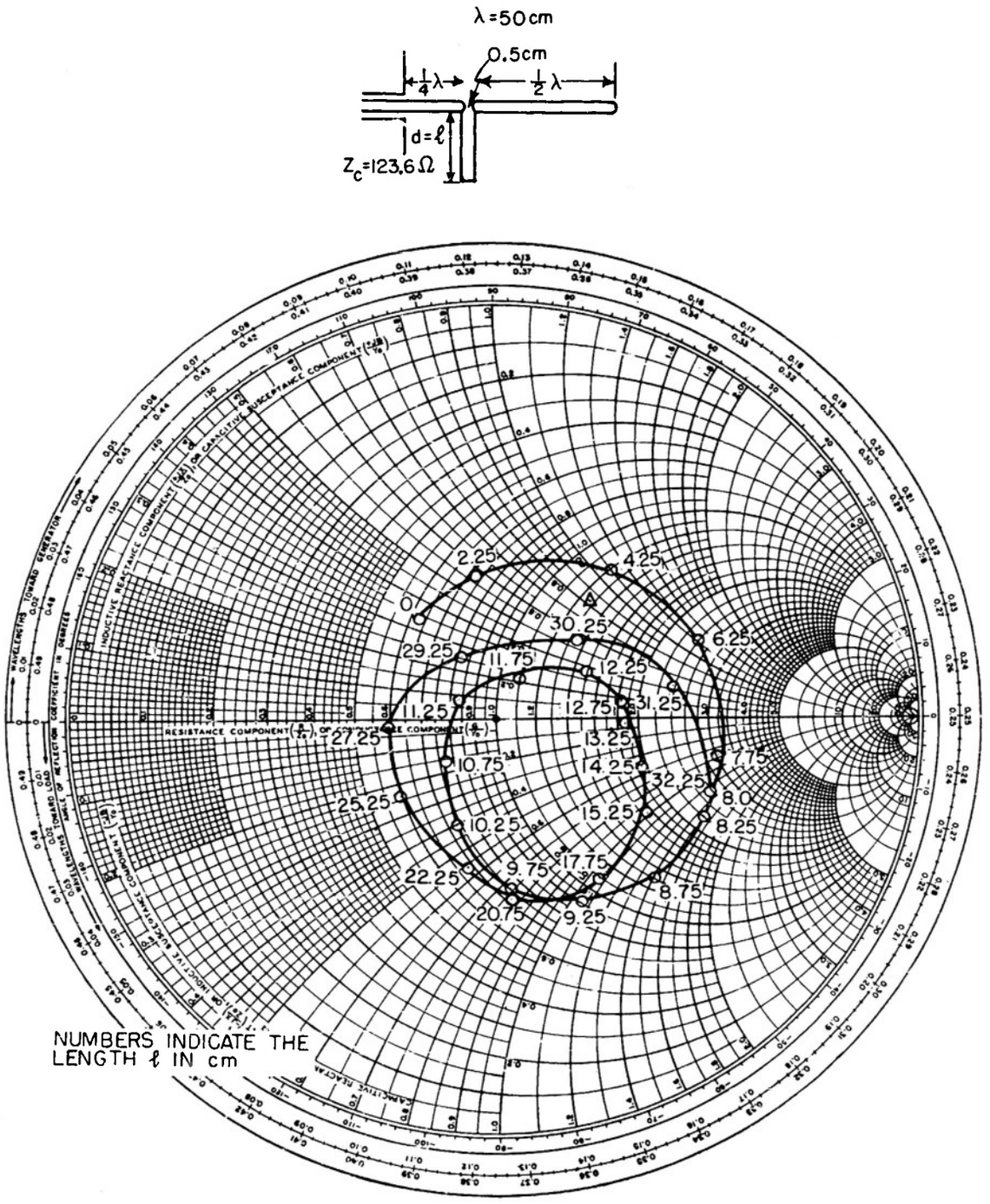

FIG.14 MEASURED IMPEDANCE OF THE COLLINEAR ARRAY WITH TWO-WIRE LINE AS COUPLING ELEMENT

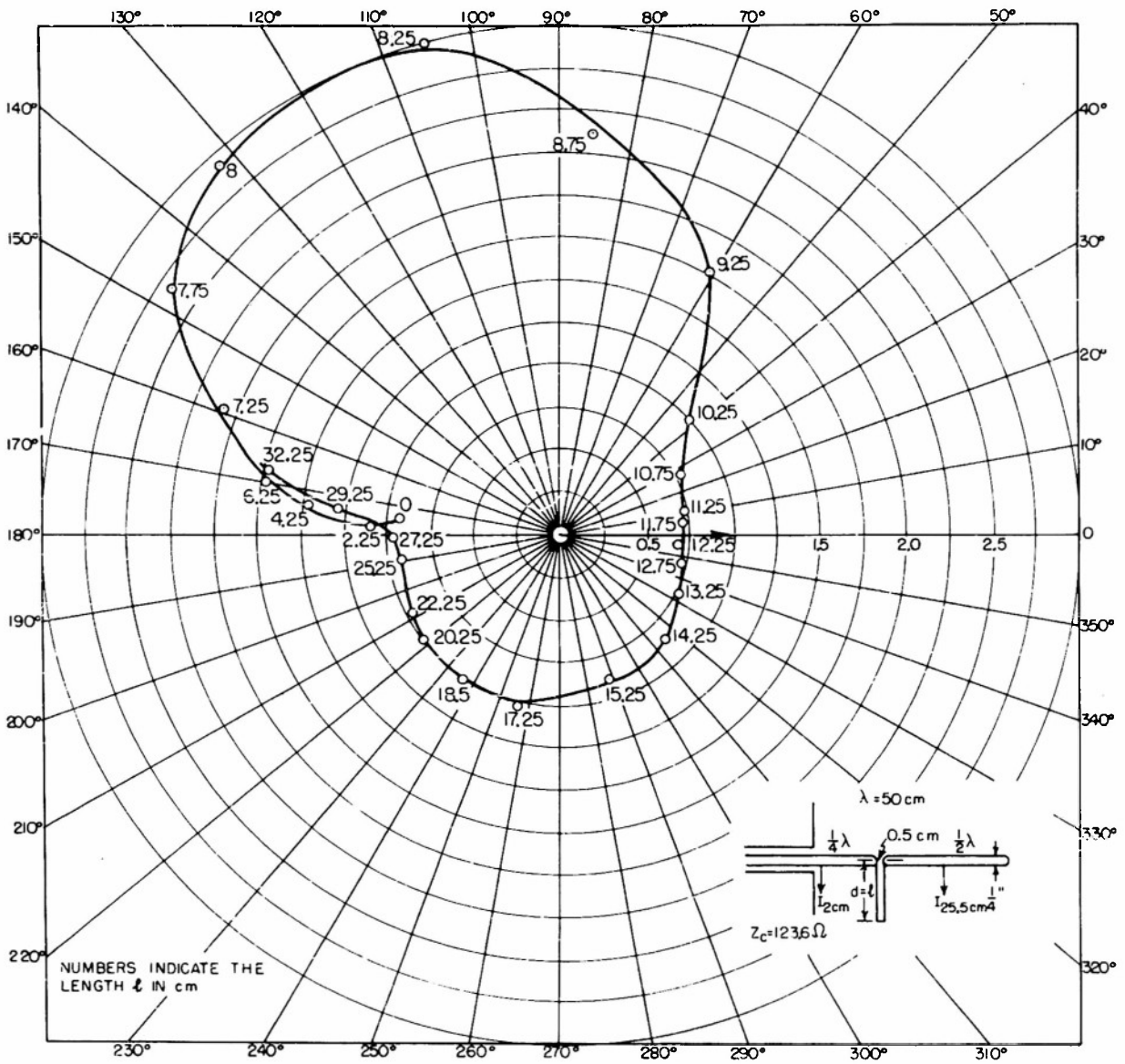

FIG.15 NORMALIZED CURRENT RATIO $\frac{I_{25.5}}{I_2}$

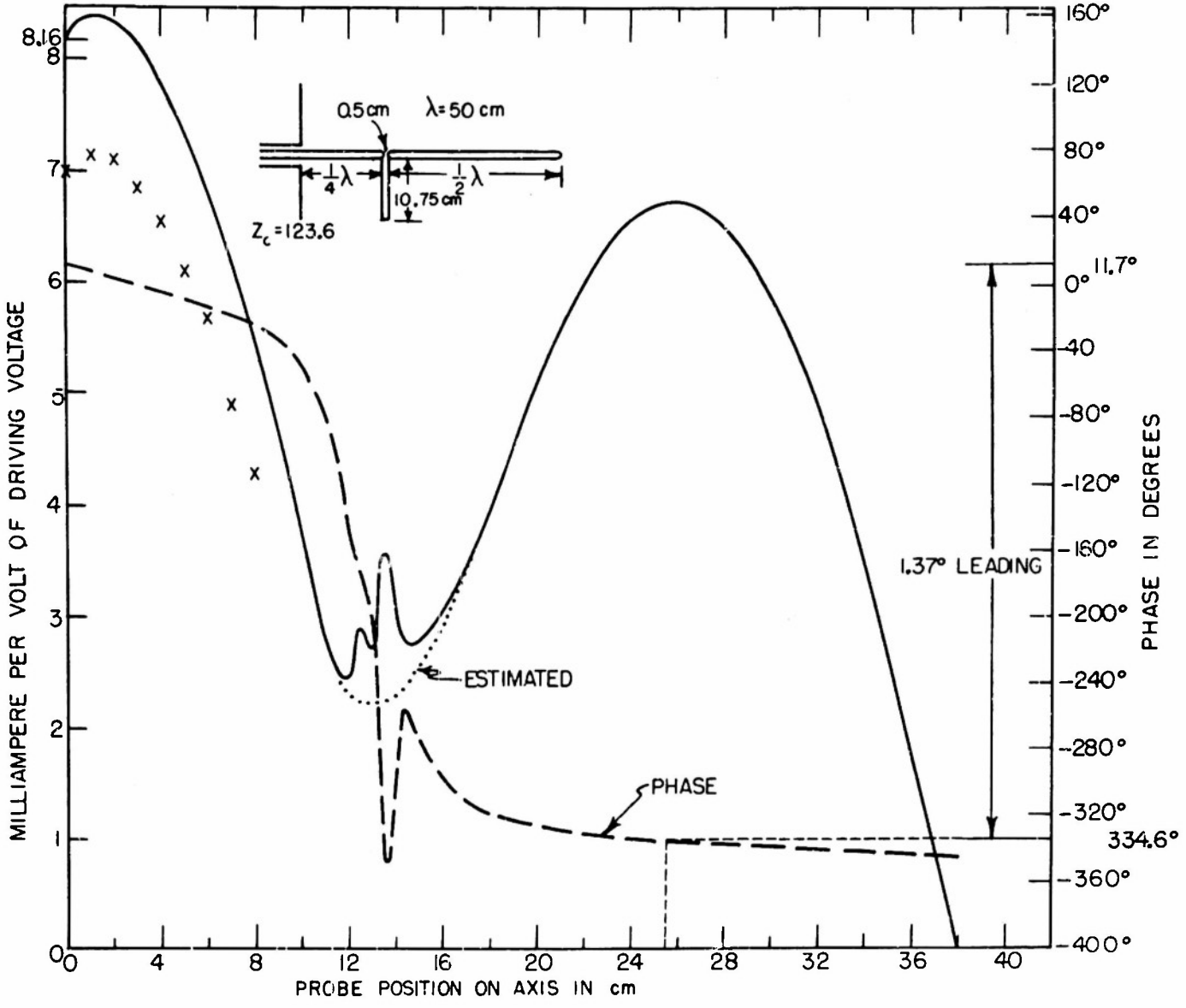

FIG. 16 MEASURED CURRENT DISTRIBUTION AND PHASE VARIATION

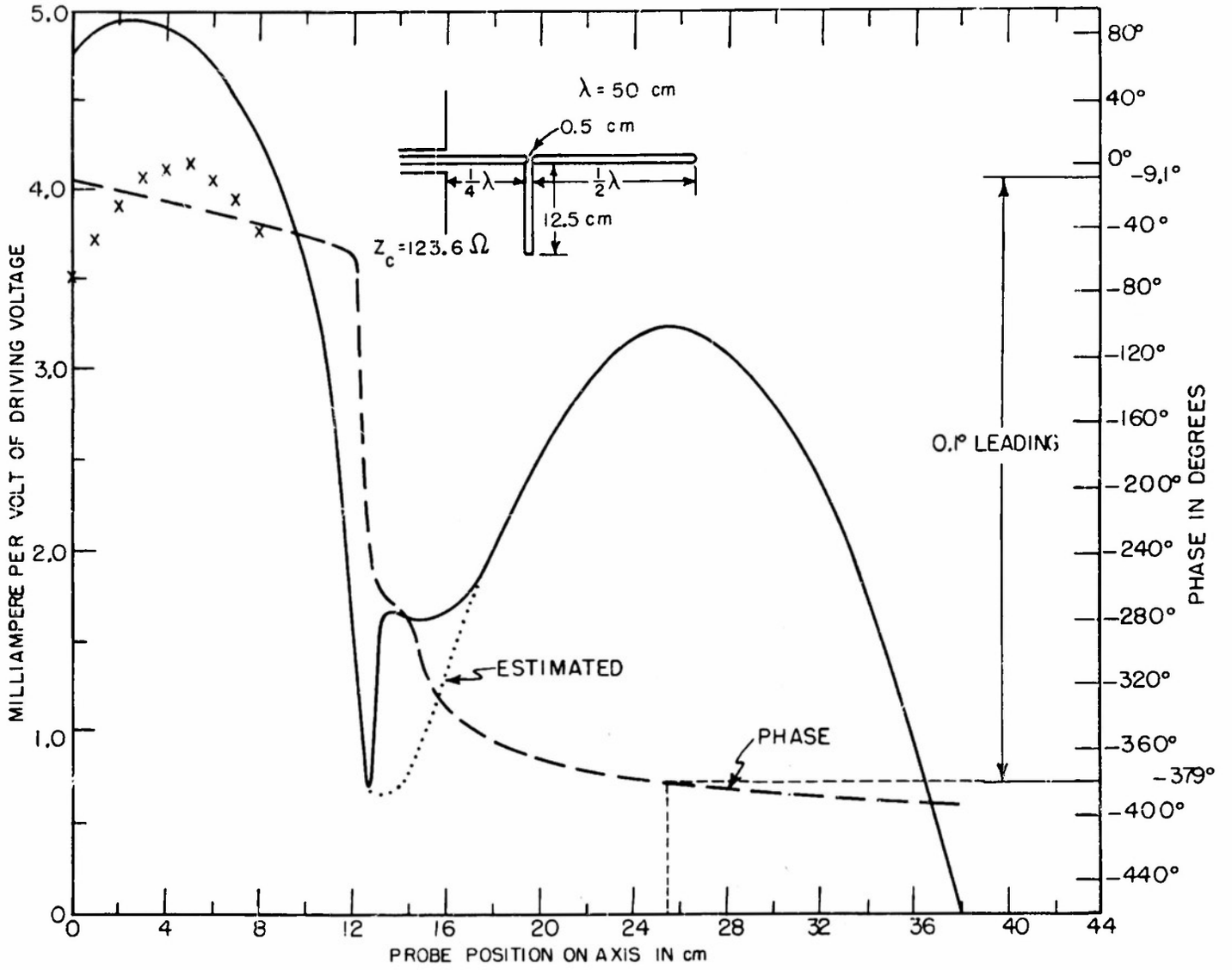

FIG. 17 MEASURED CURRENT DISTRIBUTION AND PHASE VARIATION

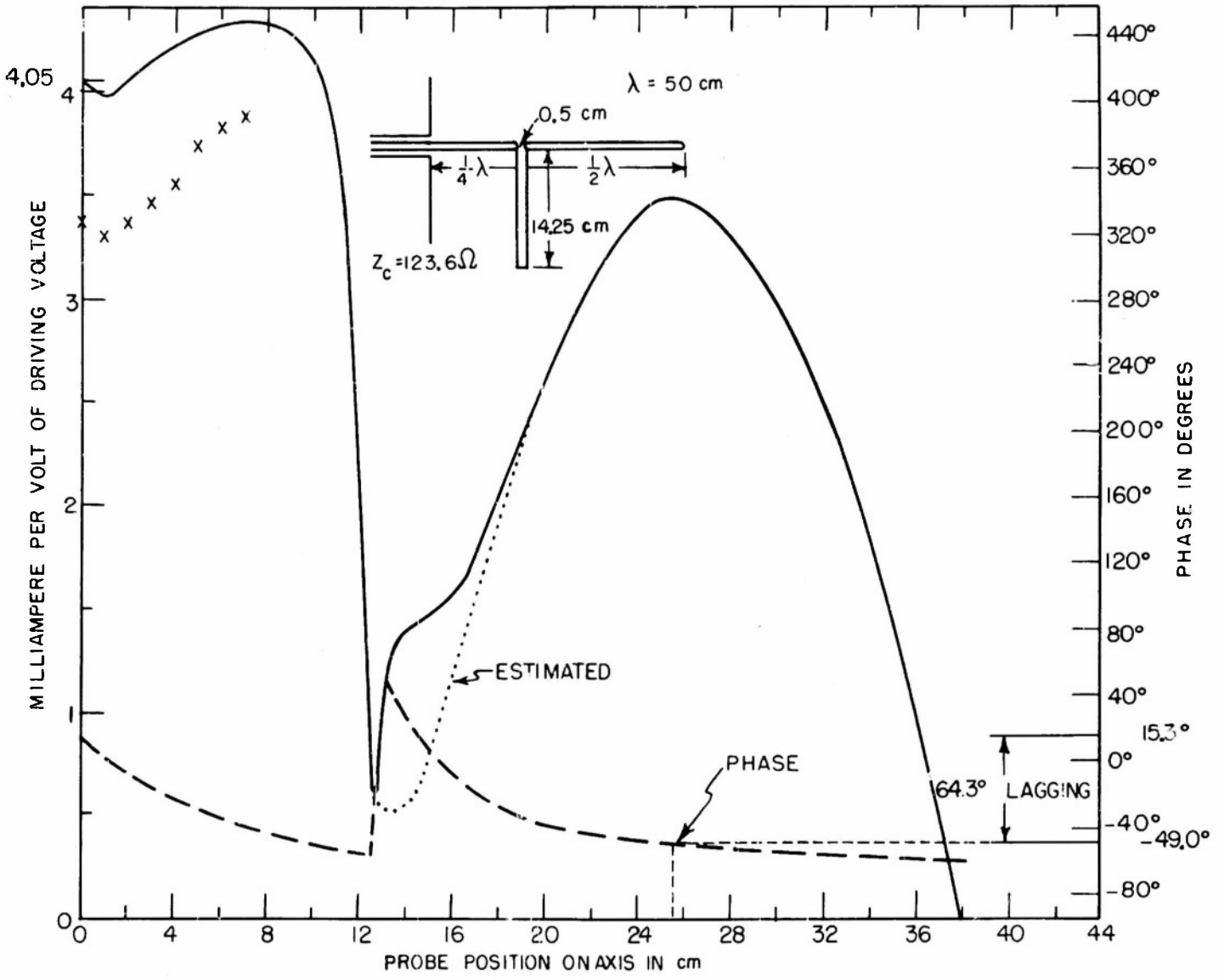

FIG. 18 MEASURED CURRENT DISTRIBUTION AND PHASE VARIATION

at the free end. When ℓ is 12.5 cm ($\frac{1}{4}\lambda$) the current at the center of the parasite is approximately in phase with that of the driving point as shown in Fig. 17. The current at the center of the parasite leads that at the driving point by 13.7 degrees for ℓ equal to 10.75 cm as shown in Fig. 16 and lags by 64.3 degrees for ℓ equal to 14.25 cm as shown in Fig. 18. (The departure of the measured curves from the expected distributions [broken lines] near the junction of the antennas and the line is considered in conjunction with Fig. 19 where this effect is most pronounced.)

The effect of the transmission-line current on the short-circuited section of the two-wire line will be discussed briefly. As long as the spacing between the two-wire line satisfies the relation $\beta_o b \ll 1$, the radiation in free space is negligibly small. On the other hand, the effect of the balanced mode on the distribution of current on the driver and the parasite may not be negligible in certain configurations. When the short-circuited section of the two-wire line is about $\frac{1}{4}\lambda$ in length, a current minimum of the balanced mode exists at the gap end (see Figs. 5(a) and (b), 12(a) and (b)); and its effect on the current distribution on the driver and parasite is negligible. When the short-circuited section of two-wire line is $\frac{1}{2}\lambda$ in length, a current maximum of the balanced mode exists at the gap (see Figs. 5(c) and (d), 12(c) and (d)). Although the balanced mode current is in a direction perpendicular to that on the parasite and driver, the close coupling at the gap modifies the current distribution on the driver and parasite near the gap. The effect of the transmission-line current on the current distribution of the parasite and driver can be seen most clearly when the two-wire line is a half-wavelength long. For this length, the current at the gap due to the antenna mode on the driver and the two-wire line is a minimum and, therefore, the effect of the transmission-line current will not be masked. The measured current distribution and phase variation for $\ell = d = \frac{1}{2}\lambda$ are shown in Fig. 19. The two sharp peaks near the gap (and the departures of the measured results in Figs. 16-18 from the broken-line curves) do not represent currents in the antennas which must follow approximately the amplitude curves in broken line. The peak in Fig. 19 may be ascribed to an intense electric field that is not perpendicular to the axis of the antenna and thus excites the shielded-loop probe. The shielded loop acts as a current probe only when the electric field is parallel to that diameter of the loop that begins at the gap in the shield. Since the electric

field at the surface of a continuous conductor is perpendicular to its surface, the gap in the shield is arranged to be at the point in the loop nearest the conductor. Since the conductor in the case of Fig. 19 is not continuous and since the charge per unit length near the end of the driver is not equal to that near the end of the outer element, the electric field near the junction of the two antennas and the section of line is not everywhere perpendicular to the axis through the antennas. As a consequence the electric field maintained by the large concentrations of charge on all conductors near this junction maintains a potential difference across the gap in the shielded loop which very much exceeds the voltage induced by the currents in the antennas. Note that these are small near the junction. Similar peaks are in Fig. 16, but they are relatively much smaller since the electric field is less intense. In Fig. 16 the charges on the adjacent ends of the antennas are opposite in sign, in Fig. 19 the same in sign. Irregularities in the shape of the curves near the junction also are observed in Figs. 17 and 18 for the same reason.

All measurements above make use of the antenna of 1/4 in. diameter. For quarter-wavelength driver it has an $\Omega = 2\ell n\frac{2h}{a} \doteq 8.7$. A very thin antenna of 0.0285 in. diameter, which for $\frac{1}{4}\lambda$ driver corresponds to an Ω of 13.1 is used for the configuration shown in Fig. 20. The measured impedance curve, when compared with that of Fig. 14 for the same configuration, but different antenna thickness, is shifted toward the high-impedance region, as it should be. The approximate analysis of the collinear array with short-circuited quarter-wavelength two-wire line as coupling element was carried out by King [5] using the superposition of the symmetrical part and the antisymmetrical part. In the symmetrical part all three units are individually center-driven by slice generators with voltages that maintain equal current in phase at the center of the units; but in the antisymmetrical part the driving voltages are so chosen that the currents at the centers of the outer units are reversed. The zeroth-order input impedance obtained by King for an infinitely thin ($\Omega \doteq \infty$) antenna array of the configuration shown in Fig. 20 with $\ell = d = \frac{1}{4}\lambda$ is equal to $\frac{1}{2}(315+j207)$ ohms, over the image plane, and is plotted as a triangular point in Fig. 20. The measured impedance for $\ell = d = \frac{1}{4}\lambda$ lies below the approximate theoretical value. The resistive parts agree very well in about the same ratio as the corresponding values for an isolated dipole but the reactive part differs con-

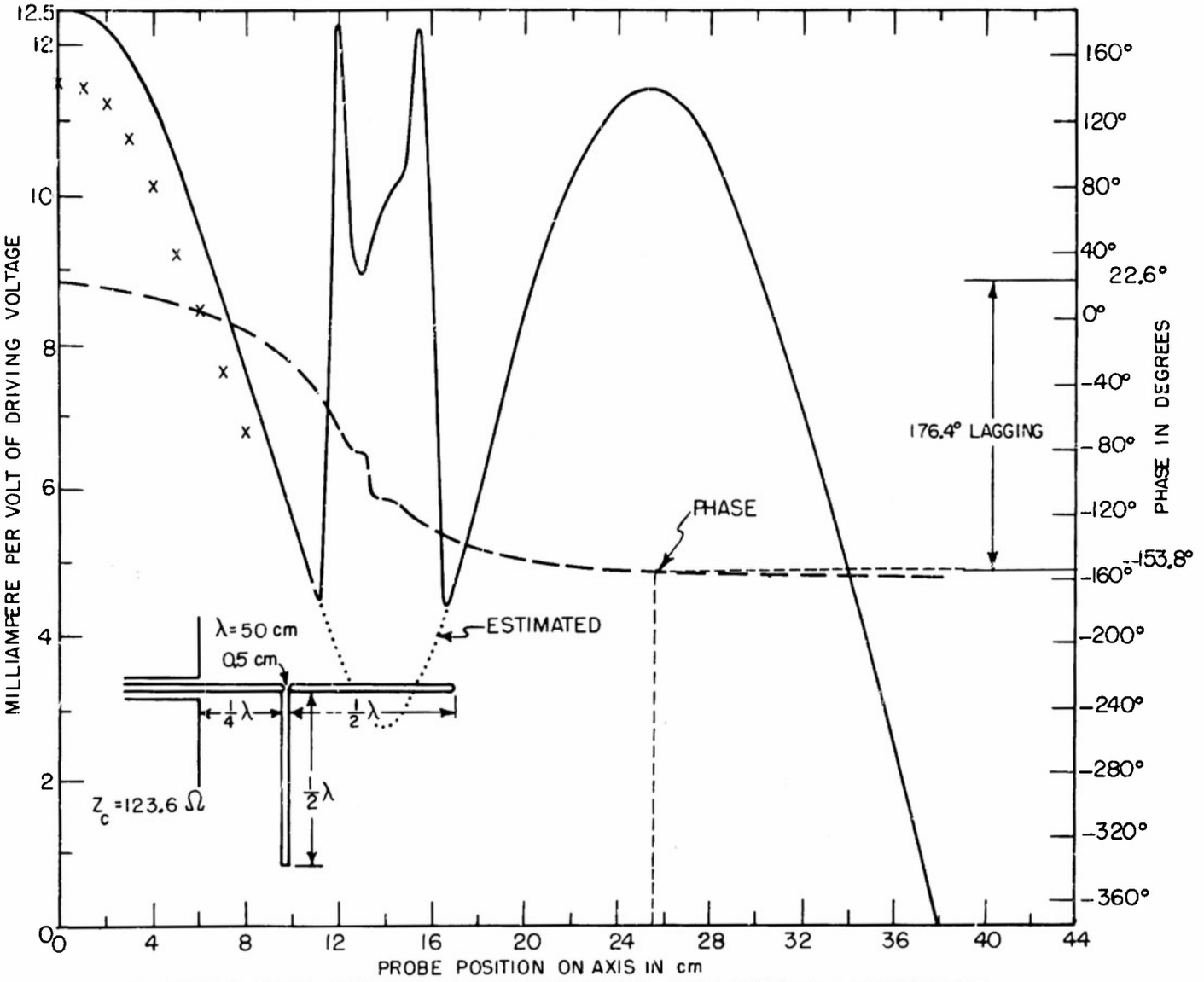

FIG. 19 MEASURED CURRENT DISTRIBUTION AND PHASE VARIATION

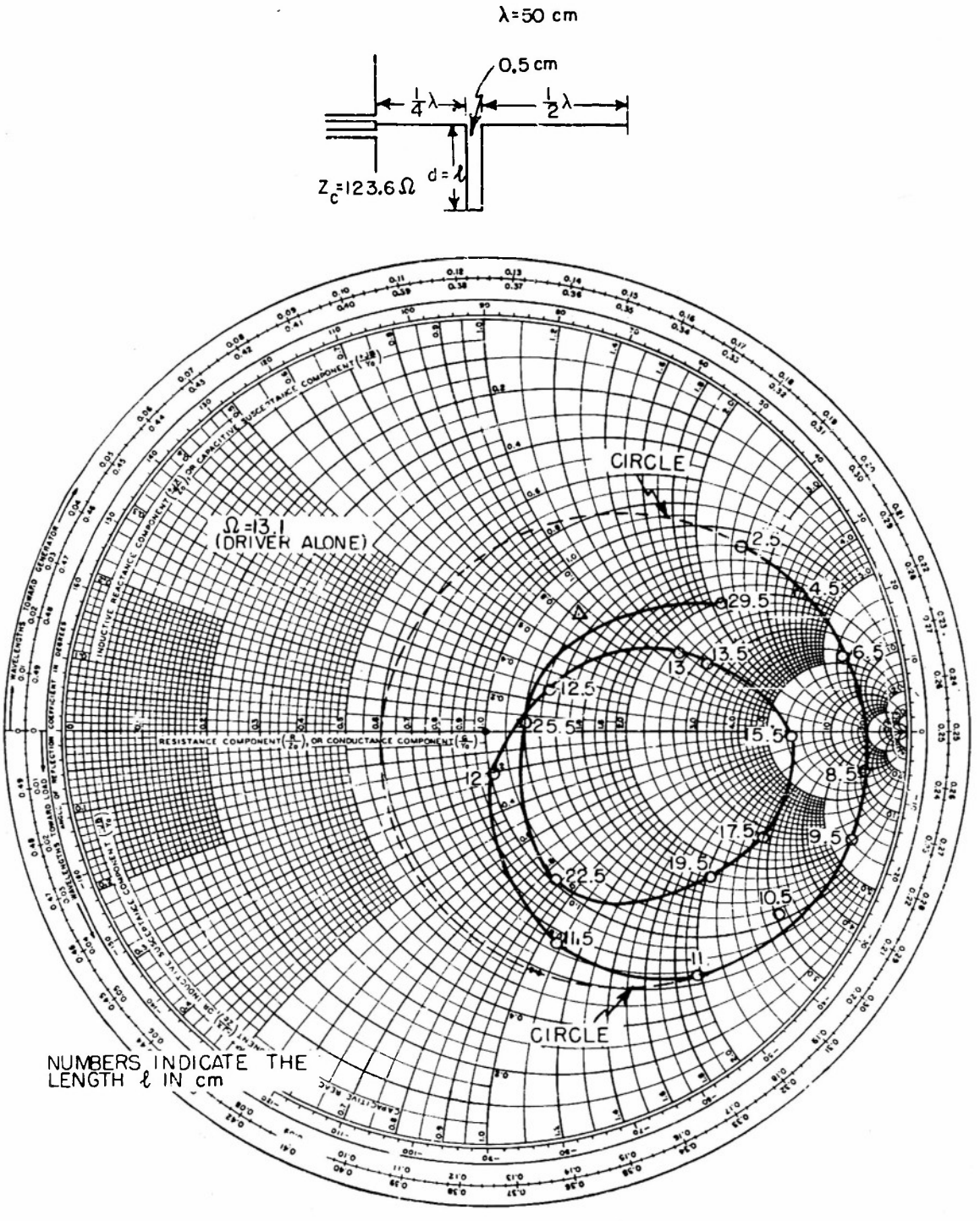

FIG. 20 MEASURED IMPEDANCE OF A VERY THIN COLLINEAR ARRAY WITH TWO-WIRE LINE AS COUPLING ELEMENT

tained by a collinear array with each element center-driven by a slice generator. These conditions are approximately satisfied in the arrangement in Fig. 16. In general, there are significant antenna currents on the section of two-wire line and the resulting field of all currents differs appreciably from that of a conventional collinear array.

Acknowledgment

The writer is indebted to Professor Ronold King for his guidance and encouragement in carrying out the experiment and his correction of the manuscript. The writer also wishes to thank Drs. Howard Andrews and Tetsu Morita for their assistance and valuable discussions.

References

1. R. King, "Theory of Collinear Antenna," J. Appl. Phys., December 1950 Cruft Laboratory Technical Report No. 121.

2. H. Andrews, "The Collinear Antenna Array," Cruft Laboratory Technical Report Nos. 176 and 177.

3. R. King, Op. cit.

4. J. Taylor, "The Sleeve Antenna," Cruft Laboratory Technical Report No. 128.

5. R. King, Op. cit.

6. H. Andrews, Op. cit.

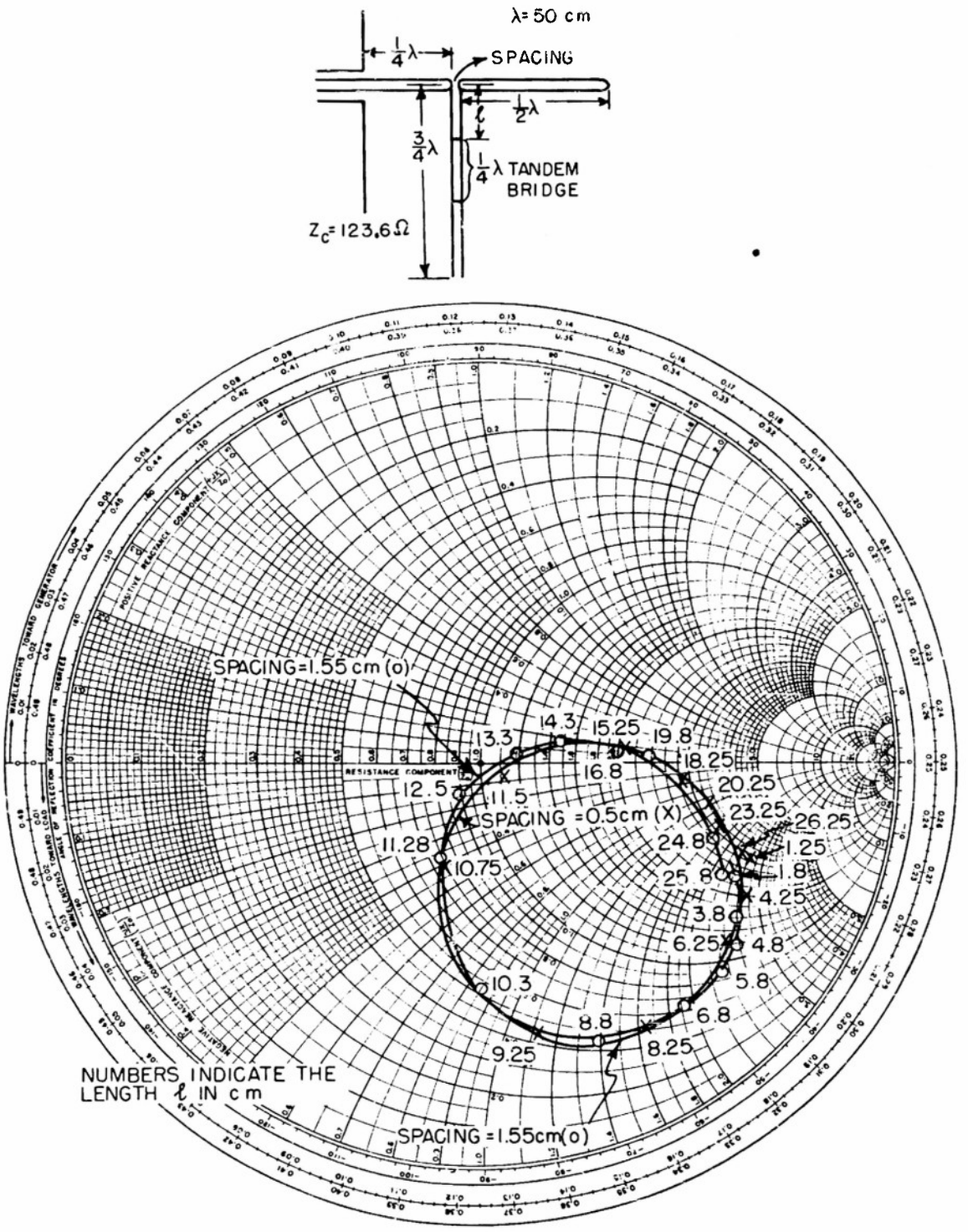

FIG.21 COMPARISON OF MEASURED IMPEDANCE OF A COLLINEAR ARRAY WITH TWO-WIRE LINE COUPLING OF DIFFERENT SPACING

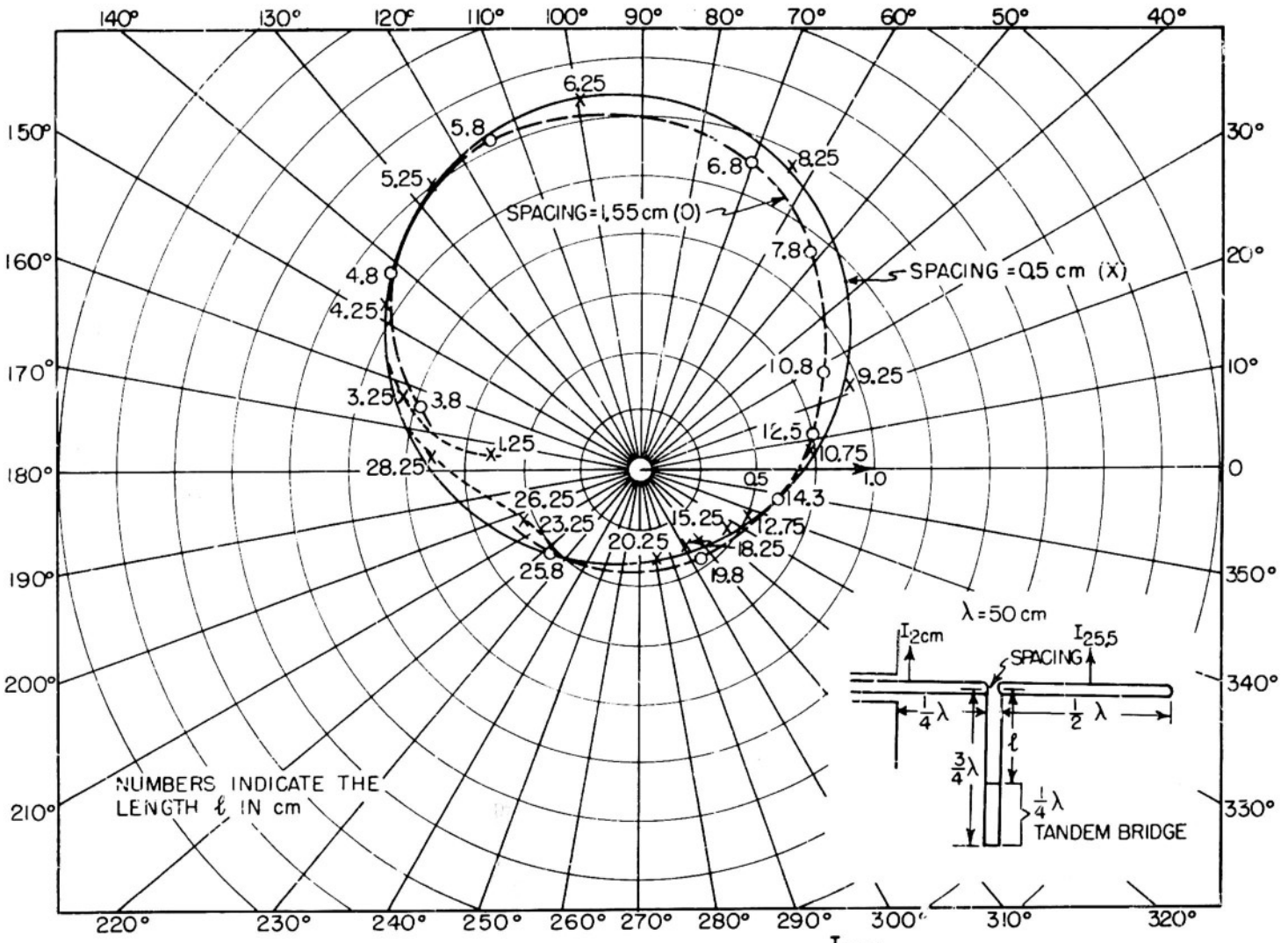

FIG. 22 COMPARISON OF NORMALIZED CURRENT RATIO $\frac{I_{25.5}}{I_2}$ FOR A COLLINEAR ARRAY WITH TWO-WIRE LINE COUPLING OF DIFFERENT SPACING

DISTRIBUTION LIST

Technical Reports

2	Chief of Naval Research (427) Department of the Navy Washington 25, D. C.
1	Chief of Naval Research(460) Department of the Navy Washington 25, D. C.
1	Chief of Naval Research (421) Department of the Navy Washington 25, D. C.
6	Director (Code 2000) Naval Research Laboratory Washington 25, D. C.
2	Commanding Officer Office of Naval Research Branch Office 150 Causeway Street Boston, Massachusetts
1	Commanding Officer Office of Naval Research Branch Office 1000 Geary Street San Francisco 9, California
1	Commanding Officer Office of Naval Research Branch Office 1030 E. Green Street Pasadena, California
1	Commanding Officer Office of Naval Research Branch Office The John Crerar Library Building 86 East Randolph Street Chicago 1, Illinois
1	Commanding Officer Office of Naval Research Branch Office 346 Broadway New York 13, New York
3	Officer-in-Charge Office of Naval Research Navy No. 100 Fleet Post Office New York, N. Y.

1	Chief, Bureau of Ordnance (Re4) Navy Department Washington 25, D. C.
1	Chief, Bureau of Ordnance (AD-3) Navy Department Washington 25, D. C.
1	Chief, Bureau of Aeronautics (EL-1) Navy Department Washington 25, D. C.
2	Chief, Bureau of Ships (810) Navy Department Washington 25, D. C.
1	Chief of Naval Operations (Op-413) Navy Department Washington 25, D. C.
1	Chief of Naval Operations (Op-20) Navy Department Washington 25, D. C.
1	Chief of Naval Operations (Op-32) Navy Department Washington 25, D. C.
1	Director Naval Ordnance Laboratory White Oak, Maryland
2	Commander U. S. Naval Electronics Laboratory San Diego, California
1	Commander (AAEL) Naval Air Development Center Johnsville, Pennsylvania
1	Librarian U. S. Naval Post Graduate School Monterey, California
50	Director Signal Corps Engineering Laboratories Evans Signal Laboratory Supply Receiving Section Building No. 42 Belmar, New Jersey

3	Commanding General (RDKRP) Air Research and Development Command Post Office Box 1395 Baltimore 3, Maryland
2	Commanding General (RDDDE) Air Research and Development Command Post Office Box 1395 Baltimore 3, Maryland
1	Commanding General (WCRR) Wright Air Development Center Wright-Patterson Air Force Base, Ohio
1	Commanding General (WCRRH) Wright Air Development Center Wright-Patterson Air Force Base, Ohio
1	Commanding General (WCRE) Wright Air Development Center Wright-Patterson Air Force Base, Ohio
2	Commanding General (WCRET) Wright Air Development Center Wright-Patterson Air Force Base, Ohio
1	Commanding General (WCREO) Wright Air Development Center Wright-Patterson Air Force Base, Ohio
2	Commanding General (WCLR) Wright Air Development Center Wright-Patterson Air Force Base, Ohio
1	Commanding General (WCLRR) Wright Air Development Center Wright-Patterson Air Force Base, Ohio
2	Technical Library Commanding General Wright Air Development Center Wright-Patterson Air Force Base, Ohio
1	Commanding General (RCREC-4C) Rome Air Development Center Griffiss Air Force Base Rome, New York
1	Commanding General (RCR) Rome Air Development Center Griffiss Air Force Base Rome, New York

2	Commanding General (RCRW) Rome Air Development Center Griffiss Air Force Base Rome, New York
6	Commanding General (CRR) Air Force Cambridge Research Center 230 Albany Street Cambridge 39, Massachusetts
1	Commanding General Technical Library Air Force Cambridge Research Center 230 Albany Street Cambridge 39, Massachusetts
2	Director Air University Library Maxwell Air Force Base, Alabama
1	Commander Patrick Air Force Base Cocoa, Florida
2	Chief, Western Division Air Research and Development Command P. O. Box 2035 Pasadena, California
1	Chief, European Office Air Research and Development Command Shell Building 60 Rue Ravenstein Brussels, Belgium
1	U. S. Coast Guard (EEE) 1300 E Street, N. W. Washington, D. C.
1	Assistant Secretary of Defense (Research and Development) Research and Development Board Department of Defense Washington 25, D. C.
5	Armed Services Technical Information Agency Document Service Center Knott Building Dayton 2, Ohio

1	Director Division 14, Librarian National Bureau of Standards Connecticut Avenue and Van Ness St., N. W.
1	Director Division 14, Librarian National Bureau of Standards Connecticut Avenue and Van Ness St., N. W.
1	Office of Technical Services Department of Commerce Washington 25, D. C.
1	Commanding Officer and Director U. S. Underwater Sound Laboratory New London, Connecticut
1	Federal Telecommunications Laboratories, Inc. Technical Library 500 Washington Avenue Nutley, New Jersey
1	Librarian Radio Corporation of America RCA Laboratories Princeton, New Jersey
1	Sperry Gyroscope Company Engineering Librarian Great Neck, L. I., New York
1	Watson Laboratories Library Red Bank, New Jersey
1	Professor E. Weber Polytechnic Institute of Brooklyn 99 Livingston Street Brooklyn 2, New York
1	University of California Department of Electrical Engineering Berkeley, California
1	Dr. E. T. Booth Hudson Laboratories 145 Palisade Street Dobbs Ferry, New York
1	Cornell University Department of Electrical Engineering Ithaca, New York

1	University of Illinois Department of Electrical Engineering Urbana, Illinois
1	Johns Hopkins University Applied Physics Laboratory Silver Spring, Maryland
1	Professor A. von Hippel Massachusetts Institute of Technology Research Laboratory for Insulation Research Cambridge, Massachusetts
1	Director Lincoln Laboratory Massachusetts Institute of Technology Cambridge 39, Massachusetts
1	Signal Corps Liaison Office Massachusetts Institute of Technology Cambridge 39, Massachusetts
1	Mr. Hewitt Massachusetts Institute of Technology Document Room Research Laboratory of Electronics Cambridge, Massachusetts
1	Stanford University Electronics Research Laboratory Stanford, California
1	Professor A. W. Straiton University of Texas Department of Electrical Engineering Austin 12, Texas
1	Yale University Department of Electrical Engineering New Haven, Connecticut
1	Mr. James F. Trosch, Administrative Aide Columbia Radiation Laboratory Columbia University 538 West 120th Street New York 27, N. Y.
1	Dr. J.V.N. Granger Stanford Research Institute Stanford, California